Engineering Geology 315 (2023) 107021

Contents lists available at ScienceDirect

Engineering Geology

journal homepage: www.elsevier.com/locate/enggeo

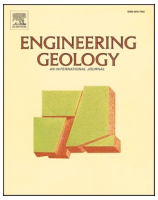

Gravity estimation of groundwater mass balance of sandy aquifers in the land subsidence-hit region of Yunlin County, Taiwan

Kuan-Hung Chen [a,b], Cheinway Hwang [a,*], Yoshiyuki Tanaka [b], Ping-Yu Chang [c]

[a] Department of Civil Engineering, National Yang Ming Chiao Tung University, 1001 Ta Hsueh Rd., Hsinchu 300, Taiwan, ROC
[b] Department of Earth and Planetary Science, The University of Tokyo, 7-3-1, Hongo, Bunkyo-ku, Tokyo 113-0033, Japan
[c] Department of Earth Sciences, National Central University, Taoyuan 320, Taiwan

ARTICLE INFO

Keywords:
Electrical resistivity imaging
Gravity change
Hydrogeology
Land subsidence
Taiwan
Water storage change

ABSTRACT

Land subsidence will decrease the safety factor of bridges and structures. Many highways and railways constructed decades ago are experiencing damage due to continual land subsidence in several alluvial fans of Taiwan. Groundwater over-pumping for industrial and agricultural uses leads to severe (>3 cm/year) land subsidence in the middle to distal Choushui River Alluvial Fan (CRAF), the largest alluvial fan in Taiwan. The Taiwan High Speed Rail passes through CRAF and land subsidence is now a major concern. Replenishing groundwater with artificial recharge lakes is a potential solution to mitigate land subsidence impacts. Using gravimetry, we examined two undetermined regional unconfined aquifers (RUAs) in the land subsidence-hit region that could host potential artificial recharge lakes to replenish groundwater. We established seven absolute gravity sites and measured time-lapsed gravity values in Yunlin in southern CRAF in 2021, including five sites in the subsidence-hit region and over two unconfined aquifers in the proximal fan. A consistent pattern of residual gravity changes associated with water storage changes at all the gravity sites confirms the recharge potential of the two RUAs in the land subsidence-hit region. Here we estimated groundwater storage changes by residual gravity changes around gravity sites without using prior hydrology information such as groundwater levels and storage coefficients. Of all the gravity sites in the land subsidence-hit region, the most significant March-to-September residual gravity change (26.6 μgal) and vertical displacement (−4.2 cm) were observed at Siutan elementary school (STES). The estimated groundwater storage change around STES is significantly large to increase the water balance in Yunlin, despite the site's severe land subsidence in 2021. We used electrical resistivity imaging (ERI) to aid the identification of the RUA near STES and discussed a potential joint gravimetry-ERI study of the RUAs for subsidence-mitigation engineering works such as constructions of recharge lakes.

1. Introduction

Mitigation of severe land subsidence (subsidence rate > 3 cm/year) is an urgent issue in Taiwan. Land subsidence in Taiwan is mainly due to excessive fluid extractions in one or multiple aquifers. The Choushui River Alluvial Fan (CRAF) is the major alluvial fan in central Taiwan experiencing land subsidence due to over-pumping. The Taiwan High Speed Rail (THSR) and several highways constructed on bridges decades ago are affected by the severe land subsidence in CRAF. Land subsidence over a region in Yunlin County covering the middle fan to the distal fan of CRAF is severe because the strata here are mainly composed of clay susceptible to compaction. THSR passes through this region, raising a concern about its safe operation here. For example, Fig. 1 shows the land subsidence rates over Yunlin County in the southern CRAF. In April 2021, the subsidence-hit region (subsidence rate > 3 cm/year) was 502.7 km^2 from the middle fan to the distal fan in the southern CRAF. The Water Resources Agency of Taiwan (WRA) proposed two methods to reduce land subsidence in regions critical to the ongoing severe subsidence. In one method, water will be injected directly into the layers experiencing compactions and responsible for the land subsidence. In the other method, sandy aquifers will be identified to safely extract groundwater from such aquifers. In both methods, the key is to detect unconfined, near-surface sandy aquifers for convenient recharge and extraction of groundwater.

* Corresponding author.
E-mail address: cheinway@nycu.edu.tw (C. Hwang).

https://doi.org/10.1016/j.enggeo.2023.107021
Received 27 July 2022; Received in revised form 11 January 2023; Accepted 23 January 2023
Available online 27 January 2023

In the face of the large hydrogeological heterogeneity of the aquifers over CRAF (Tran et al., 2022), hydraulic methods using groundwater wells for identifying sandy aquifers can be inefficient and costly. Even if a sandy aquifer is identified, its water storage capacity remains uncertain because the aquifer may lack a reliable storage coefficient. Non-intrusive methods can reduce the cost of near-surface investigations. Electrical resistivity imaging (ERI) is one of the non-intrusive methods used in hydrogeology. The ERI method has achieved some success in determining specific yield (S_y) values and groundwater levels in the proximal fan of CRAF and other areas (Chang et al., 2017; Chang et al., 2022; Dietrich et al., 2018). Another non-intrusive and efficient method for identifying regional unconfined aquifers is ground-based, time-varying gravimetry with a one-μgal precision, which has been demonstrated in several studies over Taiwan's alluvial fan (Chen et al., 2020; Chen et al., 2021b).

As shown in Van Camp et al. (2017) and other papers, a gravimeter placed on a fixed site on the ground surface may experience temporal gravity changes due to the motion of the site and the mass redistribution of the fluids around the site, including ocean and solid earth tides described in Torge (1989). Gravity values measured at a site over a land subsidence-affected area require corrections for the vertical displacements of the site before hydrogeological applications. Thus, vertical displacement measurements must be simultaneously collected when gravity measurements are collected over a site experiencing land subsidence. Gravity measurements collected in areas with small vertical displacement rates (less than a few mm/year) in the proximal fan of CRAF are typically used for determining S_y of unconfined aquifers and require no corrections for vertical movements.

In central Taiwan, including the entire CRAF, the WRA has constructed a network of groundwater wells and a network of vertical displacement-monitoring sensors that provide data to assist hydrogeological studies using gravimetry. A network of groundwater monitoring wells over CRAF provides water level data and storage coefficients over selected aquifer layers through pumping tests (Hung et al., 2012). Vertical displacements at different space and time scales over CRAF have been measured using data from leveling, GNSS, InSAR and multilayer compaction well (MLCW). The MLCW is a device installed in a single well that can monitor compactions at different depths (Hung et al., 2021). In addition, InSAR is a satellite-based method for detecting ground displacement and has been widely used over CRAF (Chen et al., 2021a; Yang et al., 2019).

Determining mass changes induced by a small amount of short-term fluid changes requires a high-precision gravimeter at the μgal level (Rosat and Hinderer, 2018). With an average accuracy of one μgal (1 μgal $= 1 \times 10^{-8}$ m/s^2) obtained over a sufficiently long measurement time, the absolute gravimeter can meet this stringent error requirement, as demonstrated in several hydrogeology studies in Taiwan and elsewhere. These studies determined hydrogeological parameters such as aquifer storage coefficient, infiltration coefficient and percolation rate at different locations in Taiwan showing hydrological processes at different temporal and spatial scales (Chen et al., 2021b). The results of gravity studies in several sandy unconfined aquifers in Taiwan showed that gravity changes range from 1 to 4 μgal during pumping tests and 1 to 26 μgal induced by inter-seasonal hydrological changes. A major monsoonal rain event can even increase the gravity value by 50 μgal in two weeks (Chen et al., 2018; Chen et al., 2021b; Chen et al., 2020).

If a gravity site is established over a sandy unconfined aquifer or a perched aquifer, gravity measurements here can be highly responsive to changes in water storage in the aquifer. In contrast, if a gravity site is over a purely confined aquifer, gravity changes at the site are expected to be much smaller. Thus, over a region dominated by confined aquifers and experiencing land subsidence, a temporary gravity site can be installed to examine if the measured gravity changes at the site are dominated by the expected land subsidence-induced gravity changes or are significantly different from such changes. If the latter is the case, the region around the gravity site may contain potential unconfined aquifers or perched aquifers, to which clean water can be injected to alleviate land subsidence near the site. As such, this gravimetric method for identifying unconfined aquifers is non-intrusive compared to intrusive methods such as drilling, which can be costly and lead to inconclusive results because the underlying aquifer may have a heterogeneous hydrogeological property. Furthermore, a joint gravimetry-ERI method can provide more hydrogeological information than a gravimetry-only or an ERI-only method.

In 2021, a major project to study methods for mitigating land subsidence in CRAF was launched by WRA and the Ministry of Science and Technology (MOST). The aim is to reduce land subsidence rates to below 3 cm/year anywhere in CRAF. The gravity team of this project was in charge of identifying potential recharge regions for further on-site testing. This study set up eight absolute gravity sites (seven in 2021 and one in 2016) in southern CRAF and measured inter-seasonal time-variable gravity values. Two sites are located in the proximal fan, four in the middle fan and two in the distal fan. With the time-lapse gravity measurements collected in 2021 and earlier at these sites, we explore the similarities and differences in gravity fluctuation patterns between these sites to understand groundwater storage potential in the subsidence-hit region and propose potential sites for facilitating recharge lakes. We expect results from this study will (1) prove the existence of unconfined

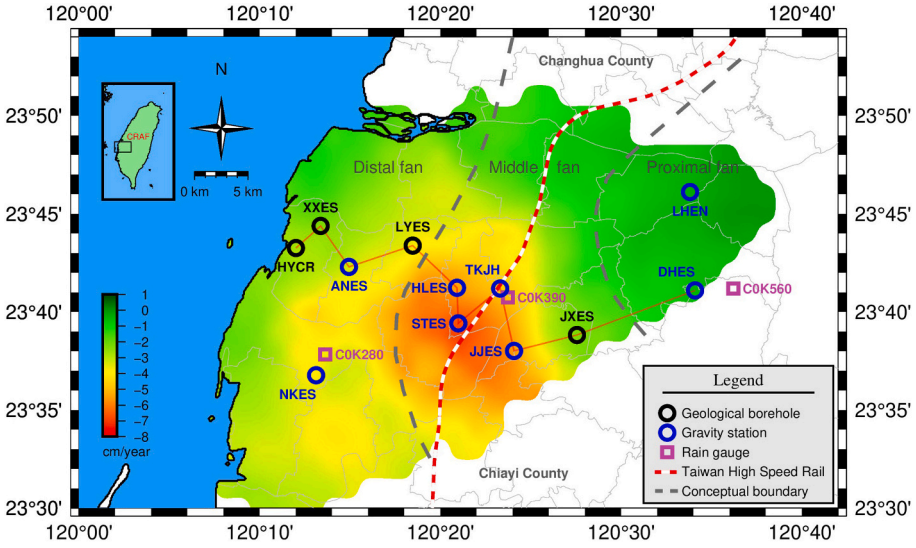

Fig. 1. Rates of vertical displacement (negative values mean land subsidence) in May 2021 from 484 leveling benchmarks in Yunlin County located in the southern Choushui River Alluvial Fan. Conceptual boundaries (the gray dash line) divide the CRAF into the proximal, middle and distal fan. The orange solid line links selected hydrogeology sites (circles) to form the hydrogeological profile in Fig. 2. Each gravity site (blue circle) is co-located with a hydrogeology site and groundwater monitoring well. Gravity sites at the middle fan to distal fan are co-located with GNSS sites and multilayer compaction wells for vertical displacement monitoring. (For interpretation of the references to colour in this figure legend, the reader is referred to the web version of this article.)

aquifers and validate their recharge potential in the land subsidence-hit region and (2) provide additional information about the retained groundwater in shallow unconfined aquifers to be considered in the mass balance estimate of the groundwater management scheme for CRAF.

2. Land subsidence and undetermined regional unconfined aquifers in Yunlin

Yunlin is located over CRAF, which is the largest alluvial fan in central Taiwan with an area of 2079 km^2. In 2021, the subsidence-hit region reached 556 km^2 over the entire CRAF. Fig. 1 shows the subsidence-affected region that occurred in the middle fan and the distal fan in southern CRAF. The long-term migrations of the Choushui River and its river branches created multiple aquifers in the aquifer system of CRAF (Fig. 2). Clay layers occurred below or near the marine facies from the middle to the distal fan, e.g., the neighborhoods of Joujoung (JJES) to Haiyuan (HYCR) in Fig. 2. Hence, few aquitards formed in the proximal fan, compared with several layers of aquitards in the middle fan which expanded to the distal fan at varying depths.

In the middle fan and distal fan of CRAF, there are three major layers of aquitards (T1 to T4), creating four confined aquifers (F1 to F4) (Fig. 2). In F1, several undetermined regional sandy aquifers are thought to exist among layers of clay created by extinct river channels. These aquifers are named “regional unconfined aquifers” (RUAs) and we will focus on RUA1 and RUA2 near gravity sites STES and JJES in this study (Fig. 2). The RUAs may have a high potential for water storage or artificial recharge. However, these RUAs were undetermined due to a lack of reliable hydrogeological parameters for the RUAs, including infiltration coefficient, infiltration rate, conductivity and storage coefficient, which are crucial for quantifying water storage. In general, the current data from hydrogeology boreholes at a few sites forming the geological profile in Fig. 2 cannot determine the extents of the RUAs and their capability.

This study will focus on the gravimetry method with a discussion on the ERI method for investigating the extent of the RUAs. The idea behind the gravimetry method is that if a RUA indeed contains groundwater-rich aquifers, there should be large seasonal variations in groundwater (or mass) storage that will create large changes in gravity values, which can be sensed by a high-precision gravimeter. In other words, if the gravity measurements at a gravity station in a subsidence-hit region experience large variations, the station is likely close to a RUA, where a groundwater facility can be constructed to recharge groundwater to reduce land subsidence. Note that there might be more RUAs in the subsidence-hit region, RUAs shown in Fig. 2 are two of the most concerned RUAs to be examined in this study.

3. Gravity data at (or close to) sites of GNSS, groundwater level and multilayer compaction measurements

Figure 1 shows the gravity sites specifically selected at sites where GNSS and groundwater wells are available. Establishing an absolute gravity site is much easier and cheaper than a groundwater monitoring well or MLCW without destroying anything. The only requirement is a solid, vibration-free foundation on which a gravimeter can be installed. In this study, a gravity site (a survey mark) was installed in a quiet room on the first floor of an existing building in a public school. We put a mark on the floor in the room for repeated absolute gravity measurements. For example, Fig. 3a and b show the gravity sites Siutan and Tuku and Fig. 3c and d show the buildings housing the rooms for the gravity sites.

At each site, we collected gravity measurements every three months to capture the gravity signals related to seasonal groundwater level

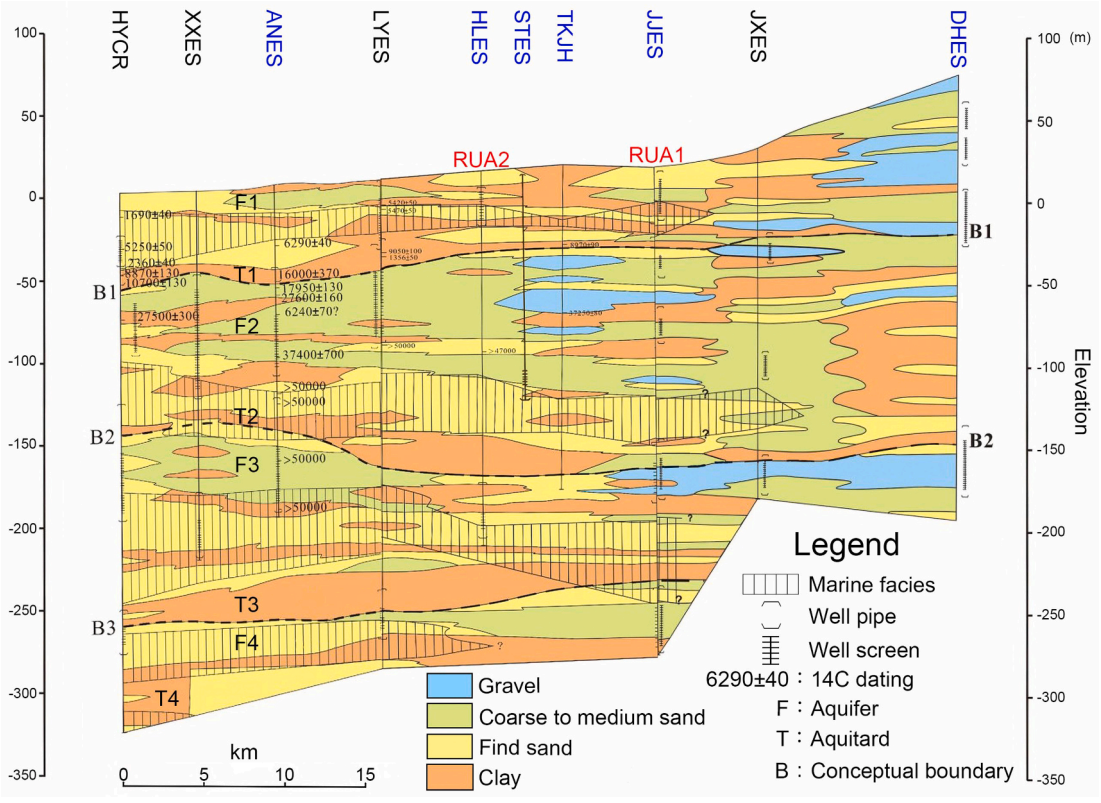

Fig. 2. Distributions of major aquifers (F1-F4) and aquitards (T1-T4) along the hydrogeological profile and gravity sites (label in blue) in this study (Fig. 1). The conceptual boundaries (B1-B3; thick horizontal dash line) drawn below aquitards T1-T3 are used to distinguish between aquifer layers. Artificial recharge lakes may be constructed near the two Regional Unconfined Aquifers (RUA1 and RUA2) investigated in this study. This hydrogeological profile is modified after Central Geology Survey (1999). (For interpretation of the references to colour in this figure legend, the reader is referred to the web version of this article.)

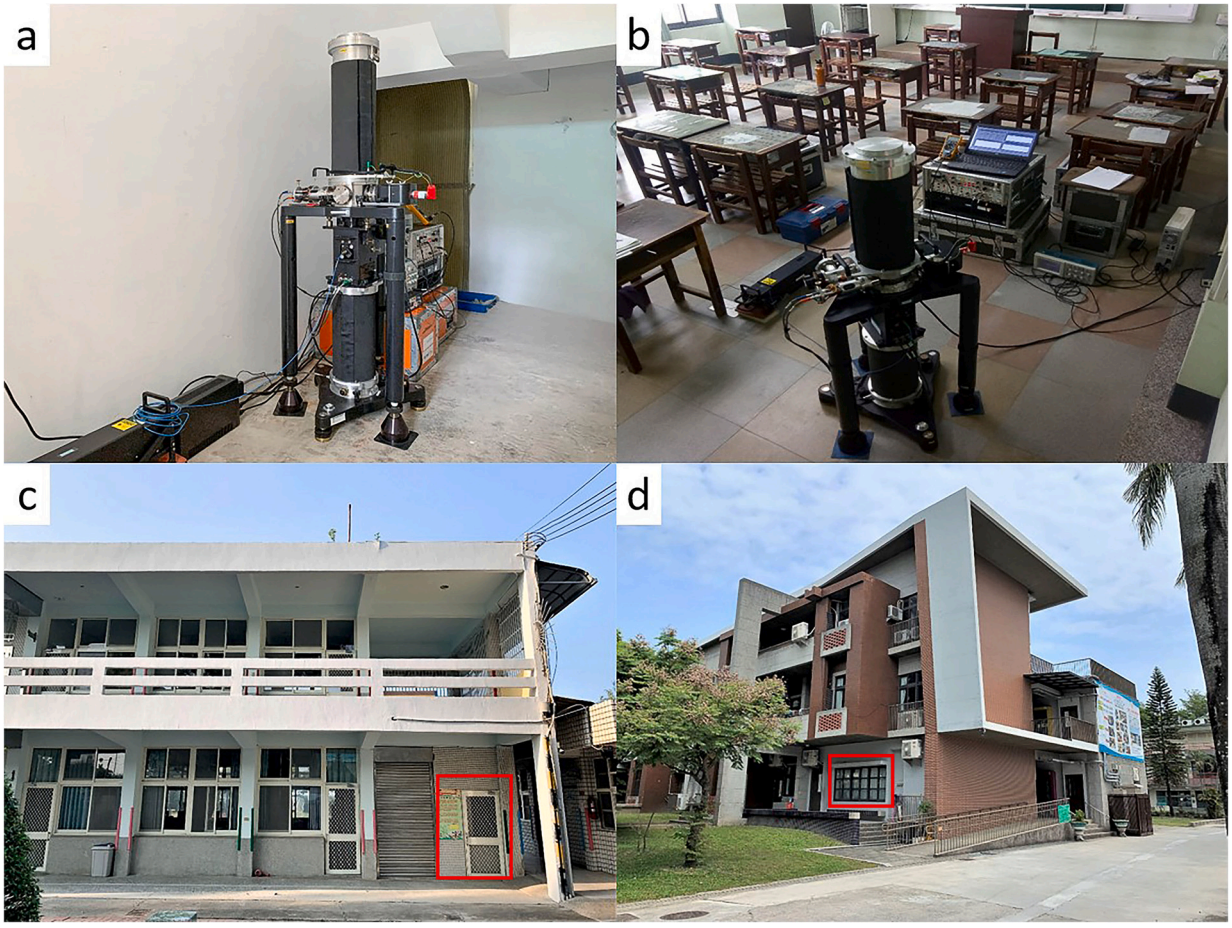

Fig. 3. Typical temporary sites for FG5 gravimeters in this study. (a) The gravity site is in a storage room below stairs at Siutan elementary school (STES) in Yunlin County. (b) The gravity site is in a classroom of the Tuku Junior High School (TKJH), with the survey mark at the joint tiles. The photo was taken on 15 April 2017. The surroundings and the building where the gravity sites (red box) is located at (c) STES and (d) TKJH. A temporary gravity site requires only an area of 1.5 m×1.5 m over a solid surface for gravity (noninvasive) measurements. (For interpretation of the references to colour in this figure legend, the reader is referred to the web version of this article.)

changes. In a year, we conducted four campaigns. In a gravity campaign at a site, we measured gravity values over a session lasting 16–20 h. To avoid vibrations and high temperatures, gravity measurements were mainly collected at nights. The two gravity measurement campaigns, one in April–May (the period with the lowest groundwater level) and another in September–October (the period with the highest groundwater level) are the most important campaigns because it is likely the difference between the two gravity values from these two campaigns is the largest among all possible differences.

All the gravity sites established in this study were co-located with groundwater monitoring wells. The groundwater levels are measured every 10 min. Table 1 shows the information on coordinates, screen depths of monitoring wells and storage coefficients used in this study at each gravity site. At least one monitoring well was co-located at each gravity site, but some sites have monitoring wells at multiple layers. Except the sites at the proximal fan, all the gravity sites were co-located with GNSS and MLCW. Using Bernese 5.2 (Yang et al., 2019), the WRA computed the daily height changes at the GNSS stations with standard errors of 3–5 mm for the height changes. Such height changes were used to determine the cumulative vertical displacements of the ground surface. On the other hand, MLCW collects monthly compactions at multiple layers up to a depth of 300 m.

At the gravity sites, we collected time-lapsed gravity measurements for the land subsidence project and for quantifying retained groundwater between two gravity measuring campaigns. Note that we use the term “retained groundwater” in this study to express the groundwater that remains in an aquifer relative to the groundwater storage at the first gravity campaign (typically in March). Thus, the actual volumes of recharge and discharge are not required. TKJH and HLES were established before 2021 for a different study than the subsidence study in this paper. There are six sites located in the land subsidence-hit regions. Four of them were in the middle fan, i.e., TKJH, HLES, STES, and JJES, and the rest of the two, ANES and NKES, were in the distal fan. We also set up two sites at the proximal fan, i.e., LHES and DHES, where the unconfined aquifers are supposed to be the major aquifers in this region. Note that gravity changes measured at LHES from 2015 to 2017 have been used for determining gravity-based S_y values (Chen et al., 2020). In addition, the Central Geology Survey (CGS) of Taiwan and the WRA conducted several pumping tests to determine storage coefficients at the selected layers and sites given in Table 1.

The sensitivity of a geophysical instrument is the primary issue to consider in acquiring field data. Gravity changes induced by water storage changes range from several to a few tens of μgal, depending on the magnitudes of hydrological events and periods of gravity measurements (Hinderer et al., 2020; Kennedy et al., 2016; Kennedy et al., 2017; Mouyen et al., 2020; Reich et al., 2019; Watlet et al., 2020). Experiences in Taiwan showed that the typical uncertainties of an absolute gravity value measured by a FG5 absolute gravimeter range from one to three μgal from hours to a day of measurements (Chen et al., 2021b), provided that corrections for the effects of solid and ocean tides, polar motion and atmospheric pressure change are properly modeled. In order to detect the μgal-level gravity changes induced by water storage changes, in this

Table 1
Information about the gravity sites, groundwater monitoring wells and storage coefficients used in this paper.

Site	Coordinates	Elevation (m)	Screen depths (m)[d]	Storage coefficient at specific depths[d]
LHEN[a]	23.7683°N, 120.5635°E	55.8	(1) 24–54	0.13
			(2) 84–114	
DHES[a]	23.6848°N, 120.5681°E	75.7	(1) 44–56	
			(2) 110–119	
TKJH[b]	23.6864°N, 120.3883°E	17.2	(1) 54–60, 66–72, 81–84 (2) 134–137, 155–158, 167–170, 176–179 (3) 218–221, 230–233, 257–263	
HLES[b]	23.6871°N, 120.3486°E	13.6	(1) 13–19, 22–31 (2) 209–218	
STES[b]	23.6569°N, 120.3497°E	13.3	(1) 120–128	
JJES[b]	23.6334°N, 120.4012°E	15.8	(1) 10–28	
			(2) 55–64	
			(3) 95–104	0.001167
			(4) 180–198	
			(5) 270–294	
ANES[c]	23.7048°N, 120.2489°E	6.2	(1) 77–92, 95–98 (2) 167–182, 188–201	
NKES[c]	23.6128°N, 120.2186°E	4.2	(1) 52–58, 62–80	0.000106
			(2) 124–142, 145–163	0.0029800

[a] Site is located in the proximal fan of CRAF.
[b] Site is located in the middle fan.
[c] Site is located in the distal fan.
[d] Screen depth and Storage coefficient at specific depths: Data provided by the Water Resources Agency and Central Geological Survey of Taiwan.

study, we employed an absolute FG5 gravimeter which can measure gravity changes at a noise level (one μgal for set gravity values) that is 3 times smaller than the gravity signals induced by water storage changes.

An absolute gravity measurement session lasting several hours results in a gravity value reflecting the average status of mass distribution during measurements. That is, the mass distribution below the absolute gravimeter is considered stable during a measurement session. Thus, in a stable environment, the gravity accuracy increases with measurement time. On the other hand, the gravity uncertainty can be greatly amplified when the hydrological status changes severely. The period of hydrological data used in this study must be consistent with the period of gravity measurements so that gravity changes can be associated with hydrological changes. Below we establish connections between measured gravity change and hydrological phenomena. In this study, the raw gravity measurements were corrected for the effects of solid and ocean tides, polar motion and atmospheric pressure change using the methods and models presented in our previous studies (Chen et al., 2020; Hwang et al., 2009).

4. Method for gravity estimation of groundwater storage change

4.1. Determining the effect of vertical displacement on measured gravity change

After applying corrections for tides, polar motion and atmospheric pressure, we can obtain a gravity change (Δg) as

$$\Delta g = g_{t_2} - g_{t_1} = \Delta g_d + \Delta g_w \quad (1)$$

where g_{t_1} and g_{t_2} are the absolute gravity values measured at times t_1 and t_2, Δg_d and Δg_w are gravity changes induced by vertical displacement and water storage change, respectively. The term Δg_d is due to the vertical motion of the site and the mass change associated with its motion. Thus, to model Δg_d at a gravity site, one must know the site's free-air gravity gradient and the density of the surface material near the site (Van Camp et al., 2017). The free-air gravity gradient is about −3.086 μgal/cm based on the GRS80 ellipsoid (Torge, 1989). However, the density can be largely unknown. Several authors used a factor to convert a measured vertical displacement to g_d, which was then removed for subsequent analyses. Torge (1989) showed that the factor can range from −1.5 to −3.5 μgal/cm and discussions on this factor (i.e. gravity change to displacement change ratio) were presented in several studies (Crossley et al., 2023; de Linage et al., 2009; De Linage et al., 2007; Van Camp et al., 2017; Wang et al., 2021). A widely adopted value for the factor is about −2.0 μgal/cm (Fukuda et al., 2016; Kao et al., 2017; Mouyen et al., 2014, 2020; Tanaka et al., 2018; Zerbini et al., 2007). Following the method used in these sample studies, we compute g_d as:

$$\Delta g_d = R_{hg} \times \Delta d \approx -2.0 \times \Delta d \quad (2)$$

where Δg_d is in μgal and Δd is vertical displacement in cm (Δd is positive in the upward direction). In engineering practice, one could use a 10%-variation for the R_{hg} value considering local density and free-air gradient, as suggested by Tanaka et al. (2018). According to Eq. 2, one centimeter of land subsidence ($\Delta d = -1$ cm) will increase the gravity value by 2.0 ± 0.2 μgal. If R_{hg} is known at a site, a measured gravity change can be converted to a vertical displacement for land subsidence studies (Beattie et al., 2021; Hwang et al., 2010).

4.2. Water storage change inferred from residual gravity change

The residual gravity change is the difference between the measured gravity change and the gravity effect due to vertical displacement (Δg_d). The residual gravity change can be used to infer water storage changes in an aquifer using approximate formulae presented below. First, the storage coefficient of an aquifer can be expressed as (Schwartz and Zhang, 2002):

$$S = b \times S_s + S_y \quad (3)$$

where b is aquifer thickness, S_s is specific storage contributing to water storage change in confined and unconfined aquifers, and S_y is specific yield defined only for unconfined aquifers. Over CRAF (F1; see Fig. 2), S_y ranges from 0.01 to 0.35 (Chen et al., 2020), S_s ranges from 10^{-3} to 10^{-6} m^{-1}, and the thickness b is on the order of 100 m. For the major confined aquifers (F2, F3 and F4; see Fig. 2), S_y is zero and S_s is on the order of the same magnitude as that of F1. The storage coefficient of an aquifer describes the percentage of water storage change when a unit hydraulic head changes in an aquifer. Eq. 3 implies that, for the same groundwater level (hydraulic head) change, the resulting storage changes in a confined aquifer and an unconfined aquifer can be substantially different due to the substantially different storage coefficients. In a confined aquifer, water storage can change in response to effective stress change due to soil skeleton deformations, which modify the water volume in the aquifer to create a gravity change. Similarly, in an unconfined aquifer, a removal or fill of water in the porous space between soil particles will introduce a dominant component of gravity change directly due to the depleted or extra water mass, and a negligible component due to skeleton deformations.

The Bouguer plate approximation for interpreting water storage change by gravimetry has been given by (Torge, 1989). Using a Bouguer plate model, we can express the relationship between a gravity change

and hydraulic head change in an aquifer as:

$$\Delta g_w = 2\pi G\rho_w \times S \times \Delta h \approx 41.9 \times S \times \Delta h \quad (4)$$

where Δg_w is the gravity change in μgal, G is the universal gravitational constant (6.67×10^{11} $m^3 \cdot kg^{-1} \cdot s^{-2}$), ρ_w is water density (1000 kg · m^{-3}), S is defined in Eq. 3 and Δh is the hydraulic head change in m. In a confined aquifer where land subsidence occurs, Δg_w could still be <1 μgal even if the storage coefficient $b \times S_s$ is 0.001 and Δh reaches 5 m. However, Δg_w can be large (>1 μgal) in an unconfined aquifer due to a large amount of drainable water released from pore space, i.e., S_y dominates the overall storage coefficient (Eq. 3).

Water storage change can be estimated from residual gravity change using the concept of equivalent water height (EWH), which is frequently used to assess the quantity of water volume in satellite gravimetry (Tapley et al., 2004; Landerer et al., 2020). In this study, the EWH (in m) change corresponding to a residual gravity change is approximated as

$$E_c = S \times \Delta h = \frac{\Delta g_w}{2\pi G\rho_w} = 0.0238 \times \Delta g_w \quad (5)$$

where Δg_w is in μgal. Using E_c, we can estimate the volume of water storage change (ΔM_w) as:

$$\Delta M_w \approx E_c \times \mathrm{A} = 0.0238 \times \Delta g_w \times \mathrm{A} \quad (6)$$

where ΔM_w is in m^3, and A is the finite area in m^2 sensed by a gravimeter. According to error propagation and considering only the random error of Δg_w, the standard deviation of ΔM_w is

$$\sigma_{\Delta M_w} = 0.0238A \times \sigma_{\Delta g_w} \quad (7)$$

where $\sigma_{\Delta g_w}$ is the standard deviation of Δg_w, which is given by

$$\sigma_{\Delta g_w} = \sqrt{\sigma_{\Delta g}^2 + \Delta d^2 \times \sigma_{R_{hg}}^2 + {R_{hg}}^2 \times \sigma_{\Delta d}^2} \quad (8)$$

where $\sigma_{\Delta g}$ is the standard deviation (error) of measured gravity change, $\sigma_{R_{hg}}$ is the standard deviation of R_{hg}, and $\sigma_{\Delta d}$ is the standard deviation of Δd. If the groundwater depth is available, then A can be approximated by a circle centered at the gravimeter site with a radius that is ten times the groundwater depth. This volume accounts for 90% of the actual groundwater volume around the gravimeter (Van Camp et al., 2017). Note that the areal sensitivity of terrestrial gravimeter, the Bouguer plate approximation and error estimation of gravity-based S_y have been thoroughly discussed in Chen et al. (2020); Kennedy et al. (2014); Pool (2008); Tsai et al. (2017).

Eq. 6 is useful for estimating the difference in groundwater volume between two epochs of gravity measurements (Table 2). For example, the difference between the gravity values measured in March and September shows how much groundwater volume (by Eq. 6) is retained right after the wet season, and this information can be an input to a water management scheme. In contrast, estimation of groundwater volume change in an aquifer typically requires hydraulic head change and storage coefficients, which are available only at limited locations and are insufficient for effective estimation of groundwater volume changes in a heterogeneous aquifer system like CRAF. In comparison, the gravity-based method (Eq. 6) requires only gravity change measurements. It is a non-intrusive method for estimating groundwater retained in a region relative to a specific epoch without requiring hydraulic head measurements and storage coefficients.

5. Results

5.1. Gravity changes in the land subsidence-hit region (middle and distal fan)

The measured gravity changes in the middle fan of CRAF are the focus of this study. We expect that vertical displacements are the major

Table 2
Gravity change, vertical displacements, and groundwater levels on the dates of gravity measurements.

Site	Date	Gravity change (μgal)[a]	Std. dev. (μgal)	Vertical displacement (m)[b]	Water level height (m)[c]
LHEN	3/7/2021	0 (978,817,658.1)	1.3		34.26
	5/20/2021	−10	0.9		32.70
	9/24/2021	34.6	1.7		40.54
	11/21/2021	23.5	0.9		39.04
DHES	5/12/2021	0 (978,810,321.6)	0.9		52.01
	9/22/2021	25.4	1.0		69.13
TKJH	11/28/2015	0 (978,843,309.7)	1.58	0 (40.779)	4.38
	5/7/2016	1.4	1.18	−0.018	3.96
	10/15/2016	7.8	3.21	−0.014	7.00
	4/15/2017	18.8	2.1	−0.057	−0.51
	3/6/2021	0 (978,843,365.0)	1.7	0 (40.548)	−2.31
	5/15/2021	−3.6	1.4	−0.024	−5.86
	9/25/2021	15.4	3.1	−0.023	1.53
	10/20/2021	10.2	4.0	−0.031	1.10
HLES	12/1/2015	0 (978,851,778.5)	2.4	0 (36.989)	9.18
	5/9/2016	3.7	3.3	−0.026	7.18
	10/21/2016	17.8	3.0	−0.028	9.23
	4/17/2017	17.3	1.3	−0.074	7.42
STES	3/4/2021	0 (978,849,653.3)	1.7	0 (38.555)	−10.84
	5/19/2021	10.5	1.6	−0.056	−15.87
	9/23/2021	35.0	1.4	−0.042	−5.16
	11/18/2021	21.3	3.4	−0.048	−5.80
JJES	3/15/2021	0 (978,839,643.6)	1.8	0 (39.649)	11.35
	5/14/2021	12.1	1.6	−0.048	10.34
	9/24/2021	22.6	1.0	−0.042	12.25
	10/19/2021	14.7	4.0	−0.045	12.46
ANES	3/8/2021	0 (978,870,135.1)	2.0	0 (29.422)	−14.39
	5/17/2021	−3.4	1.4	−0.023	−18.41
	11/17/2021	8.97	4.8	−0.023	−12.60
NKES	3/9/2021	0 (978,864,235.5)	2.0	0 (27.700)	−21.38
	5/18/2021	7.1	2.1	−0.042	−26.93

(continued on next page)

Table 2 (*continued*)

Site	Date	Gravity change (μgal)[a]	Std. dev. (μgal)	Vertical displacement (m)[b]	Water level height (m)[c]
	9/29/2021	27.9	2.1	−0.020	−14.64
	11/16/2021	20.2	4.5	−0.029	−16.68

[a] Gravity change: Values are relative to the first gravity measurement. The absolute gravity value is provided in the column of the first measurement at each site.

[b] Vertical displacement: Values are relative to the first measurement. The ellipsoid height of the GNSS antenna is provided in the column of the first measurement at each site. The standard error of daily vertical displacement is about 7 mm on average.

[c] Water level height: Elevation of groundwater level from the shallowest monitoring well (Table 1).

contributors to the gravity changes, but it turns out water storage changes in the RUAs made another important contributor. For example, the gravity values increased by 15 μgal from March to September 2021 at TKJH in Fig. 4 and Table 2, which cannot be explained by the 2.3-cm vertical displacement using Eq. 2. In addition, gravity changes from March to May 2021 were 10 μgal at STES and 12 μgal at JJES, which were 3 to 4 times more than those at TKJH. However, vertical displacements were about twice that at TKJH in the same period (Fig. 5 and Table 2). These unexpected results allow us to examine the potential of the RUAs in retaining groundwater after the wet season.

To supplement the identification of two RUAs in Yunlin's subsidence-hit region (Section 5.4), here we examine the patterns of gravity changes in the proximal fan of CRAF at gravity sites LHEN and DHES, where water storage changes in the unconfined aquifers near the sites dominate gravity changes. The two sites are located in the proximal fan of CRAF, where the nearest GNSS site LNJH shows that the rate of vertical displacement was 5 mm/yr. Therefore, the average gravity change induced by monthly vertical displacements is <1 μgal, which is smaller than the measurement precision of the absolute gravimeters FG5 used in this study.

Figure 6 shows the gravity changes and hydrological records at LHEN and DHES in 2021. The precipitation records are from site C0K280, which is 5 km east of DHES. The gravity changes at LHEN and DHES are coherent with the precipitation records and groundwater level changes. Like the four gravity sites in the subsidence-hit region of Yunlin (Fig. 5), gravity changes increased at DHES and LHEN after intensive precipitation in the end of May 2021. The similar patterns of gravity changes in the proximal fan and subsidence-hit region (Fig. 4 and Fig. 6) indirectly confirmed the existence of two RUAs in the middle fan and other potential RUAs near some gravity sites established in this study.

Comparisons between different gravity sites and different years also show some interesting inconsistencies in gravity changes. Table 2 shows all the gravity changes, vertical displacements and groundwater level changes measured in this study. All the time-variable values are relative to the first measurement at each site. First, the gravity change at HLEN was twice that at TKJH in the end of the wet season in 2016, although the height changes were almost the same (Fig. 4, Fig. 5 and Table 2). At HLEN, the gravity value increased by 14 μgal from May to October 2016, compared with 6 μgal at TKJH. In addition, the measured gravity changes at TKJH and HLEN had different patterns from October 2016 to April 2017. The gravity values at HLEN remained stable but increased to 11 μgal at TKJH.

Second, we notice a clear gravity decrease within one to two months

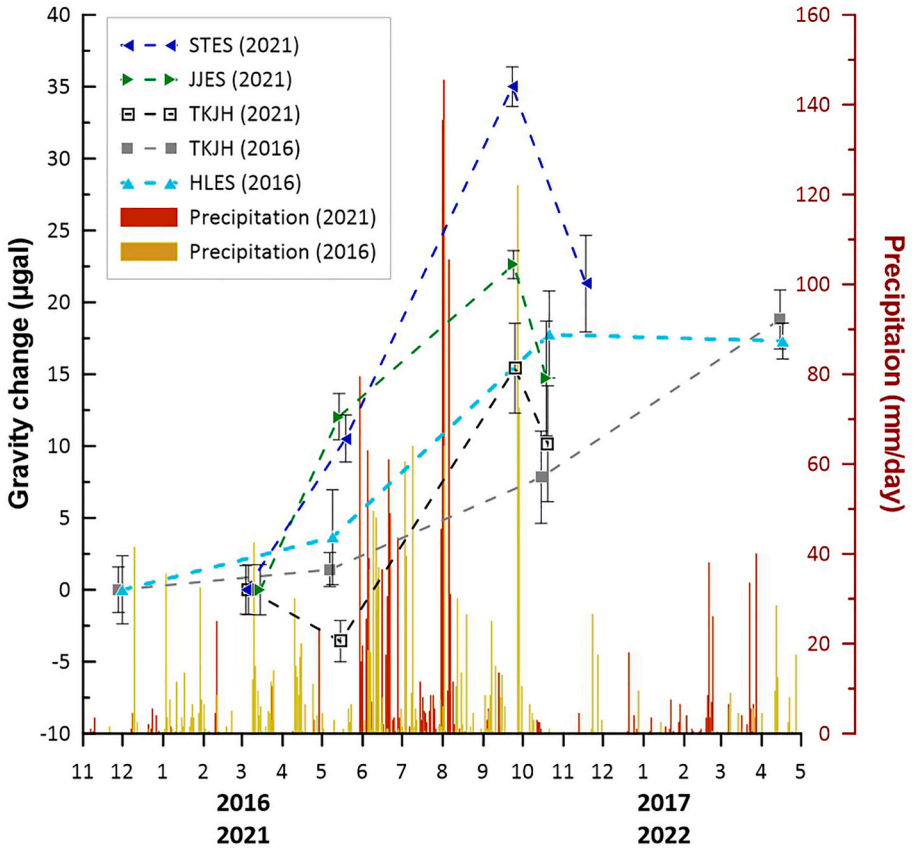

Fig. 4. Gravity changes at four sites from November to May in 2016 and/or 2021 and daily precipitation at C0K390 (co-located with TKJH) in the middle fan. The gravity changes are relative to the first measurements at each site.

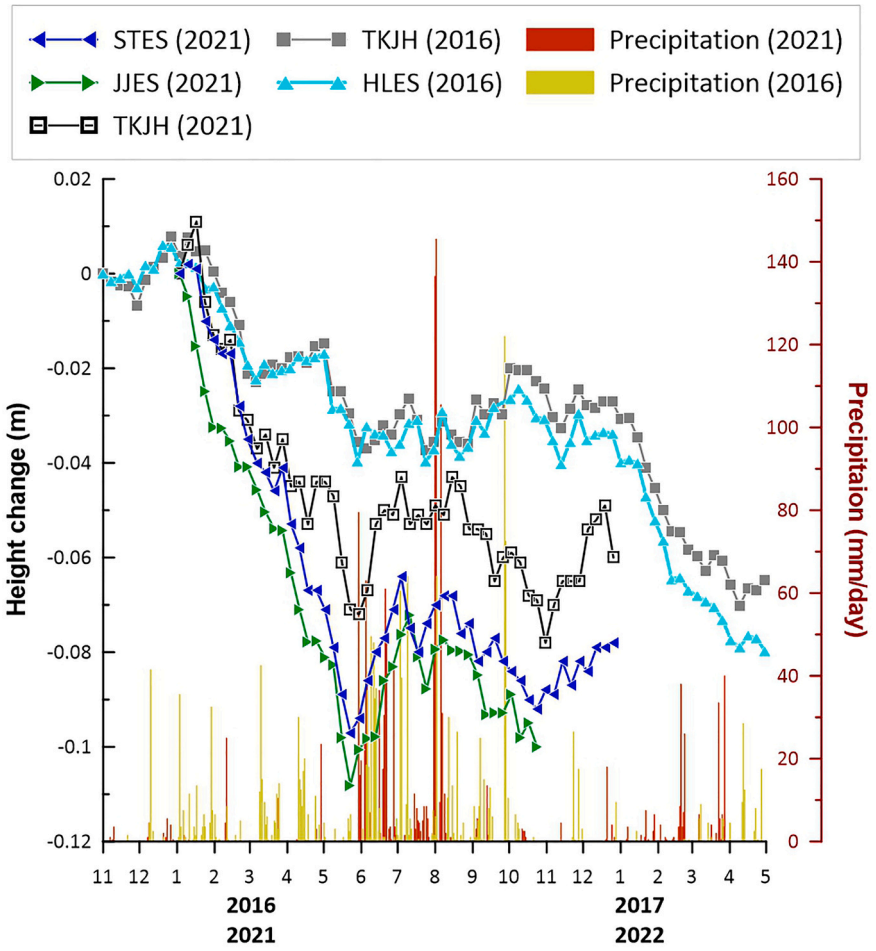

Fig. 5. Vertical displacements and precipitation records in the middle fan at four gravity sites in 2016 and 2021. The daily precipitation was collected from the rain gauge at C0K390 (Fig. 1), which is co-located with the TKJH gravity site.

right after the wet season in 2021, but land subsidence persisted. Another unexpected gravity decrease occurred at TKJH from March to May 2021, when aquifer layer compactions were ongoing. A similar pattern of gravity change was also shown in Fig. 7. NKES experienced a vertical displacement twice that at ANES, but the gravity value varied in the opposite direction from March to May 2021.

Third, the pattern of positive gravity change at NKES is similar to that at JJES and STES (Figs. 4 and Fig. 7). However, only 7-μgal gravity increase was detected at NKES, where the vertical displacement was 4 cm, compared to 5 cm at STES and JJES from March to May 2021. On the other hand, ANES showed a negative gravity change as TKJH from March to May 2021. Note that the gravity value at ANES in September was not measured due to a FG5 maintenance. ANES could also experience a negative gravity change similar to the rest of the sites in the land subsidence-hit region.

5.2. *Gravity contribution from vertical displacements*

Table 3 shows gravity contributions from vertical displacements for each gravity measurement relative to the first measurement at each site using Eq. 2. The vertical displacement (Δd) in Eq. 2 was derived from GNSS measurements at each gravity-GNSS co-located station in this study. Therefore, we first present the results of vertical displacement at STES, TKJH, JJES and HLES, which underwent seasonal oscillations that were highly correlated to precipitation (Fig. 5). Seasonal oscillations of ground surface and their relationships to changes in precipitation and groundwater level over CRAF were also shown in Lu et al. (2020). Note that the GNSS-observed heights at TKJH in the first week of 2016 and 2021 are 40.779 m and 40.584 m, respectively (Table 2).

At station TKJH, the height changes in 2016–2017 and 2021–2022 are also plotted to show the contrast in height changes between the regular year 2016 and the drought year 2021. Fig. 5 also shows the precipitation records in 2016 and 2021 at C0K390, which is co-located with the gravity site, groundwater monitoring wells and MLCW at TKJH. There are sharp differences in vertical displacement between 2016 and 2021 at TKJH. In the first half of 2021, Taiwan experienced a severe drought, leading to a land subsidence rate of 6.7 cm/year in May 2021 at TKJH, which was 1.8 times that of 2016. Typically, land subsidence in Yunlin persisted until a major precipitation event occurred in late May. However, in 2016 there was a significant rebound from March to April 2016 at TKJH and HLES because 2016 is a year with persistent rain.

Over CRAF, a typical wet season lasts from late May to September, during which stationary fronts in late May and typhoons in July–September bring intensive precipitation. A typical dry season lasts from October to early May, with far less precipitation than the wet season. However, the occurrences of stationary fronts, typhoons and thus heavy rains are unpredictable. For instance, three severe typhoons passed through Taiwan from July to September in 2016, but only one typhoon occurred in 2021. Therefore, the amounts of precipitation can vary from one wet season to another, leading to interannual rain changes for 2016 and 2021. The year 2016 had a regular wet season, but 2021's wet season received very little rain and thus 2021 was a year of exceptional drought, which put Taiwan's water management system to the test. In 2016, the precipitation was abundant throughout the year, not only in the wet season. In contrast, 90% of precipitation fell in the wet season of 2021, with only 10% of rain from the dry season. As a result of little rain

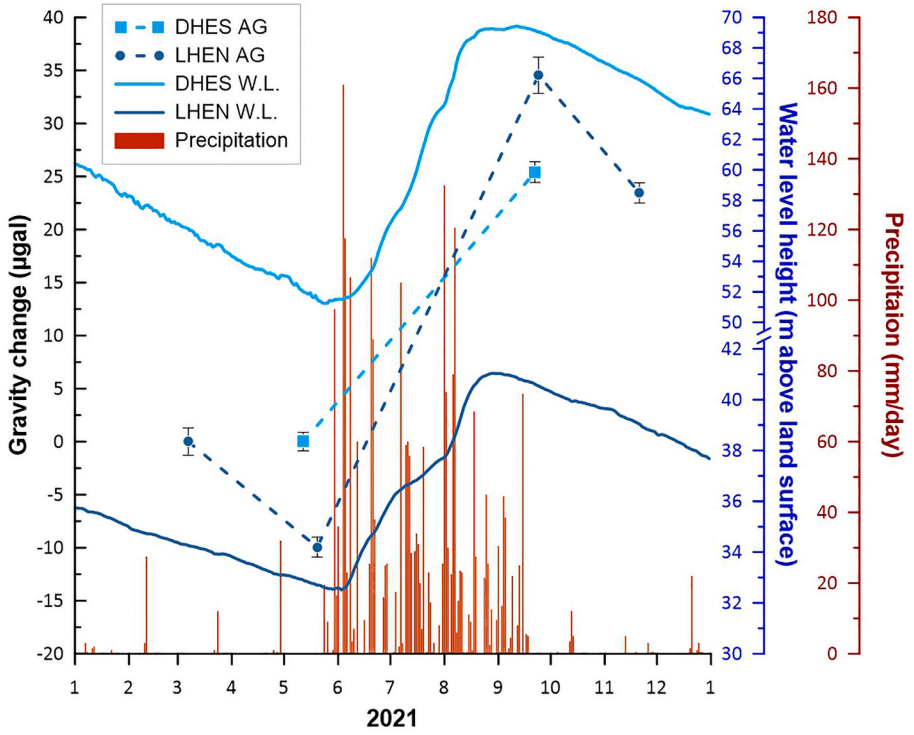

Fig. 6. Gravity changes and water level height changes at gravity sites LHEN and DHES (proximal fans) in 2021. The water level heights in this figure represent the shallowest groundwater monitoring well at each site, which are DHES_D44–54 and LHEN_D24–54 (Table 1). The daily precipitation was collected from the rain gauge at C0K560 (Fig. 1).

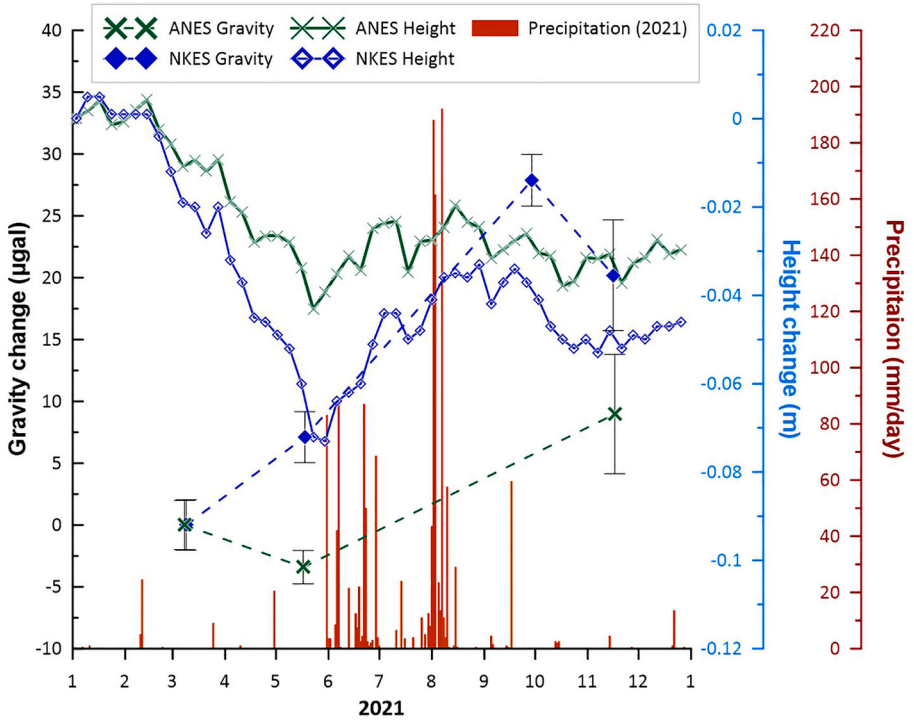

Fig. 7. Gravity changes and surface height change at gravity sites in the distal fan in 2021. The daily precipitation was collected at the C0K280 rain gauge (Fig. 1).

in the dry season of 2021, 2021 experienced a large land subsidence rate, which was twice that in 2016 at all sites.

In general, the ground surface height is relatively high in the wet season but remains stable from October to December. Aquifer compaction starts around January and continues through May until a major stationary front occurs in late May. About 20% of accumulated compression in the dry season might rebound in the wet season. If there is sufficient precipitation after September, the land surface will fluctuate by a small range, as seen in 2016. However, the ground surface height may again reach its lowest level and become even lower if the

Table 3
Contributions to the measured gravity changes from vertical displacement, confined aquifer and residual gravity.

Site	Date	Vertical displacement (μgal)[a]	Confined aquifers (μgal)[b]	Residual gravity(μgal)[c]
LHEN	3/7/2021	0	0	0
	5/20/2021			−10
	9/24/2021			34.6
	11/21/2021			23.5
DHES	5/12/2021	0	0	0
	9/22/2021			25.4
TKJH	11/28/2015	0	0	0
	5/7/2016	3.6	−0.01	−2.2
	10/15/2016	2.8	0.15	5
	4/15/2017	11.8	−0.27	7
	3/6/2021	0	0	0
	5/15/2021	4.8	−0.20	−8.4
	9/25/2021	4.6	0.21	10.8
	10/20/2021	6.2	0.19	4
HLES	12/1/2015	0	0	0
	5/9/2016	5.2	−0.01	−1.5
	10/21/2016	5.6	0.02	12.2
	4/17/2017	14.8	−0.05	2.5
STES	3/4/2021	0	0	0
	5/19/2021	11.2	−0.25	−0.7
	9/23/2021	8.4	0.28	26.6
	11/18/2021	9.6	0.25	11.7
JJES	3/15/2021	0	0	0
	5/14/2021	9.6	−0.27	2.5
	9/24/2021	8.4	0.30	14.2
	10/19/2021	9.0	0.30	5.7
ANES	3/8/2021	0	0	0
	5/17/2021	4.6	−0.03	−8
	11/17/2021	4.6	0.008	4.37
NKES	3/9/2021	0	0	0
	5/18/2021	8.4	−0.02	−1.3
	9/29/2021	4.0	0.03	23.9
	11/16/2021	5.8	0.02	14.4

[a] Vertical displacement: Gravity change estimated by vertical displacement relative to the first measurement (Table 2) using Eq. 2 at each site. A positive value means the gravity value was increased due to land subsidence.

[b] Confined aquifers: Summation of gravity change estimated by groundwater level change in confined aquifers (Table 1) relative to the first measurement using Eq. 3 at each site. A positive value means the gravity value was increased due to increasing groundwater storage.

[c] Residuals gravity: Values are calculated as Gravity change (μgal) in Table 2 minus Vertical displacement (μgal) in Table 3, regardless of the estimated value in Confined aquifers (μgal) in this table, considering the measurement Std. (μgal) of gravity in Table 2. A positive value means the groundwater storage was increased relative to the first measurement at each site.

groundwater recharge to aquifers is scarce after the wet season.

5.3. Gravity contribution from confined aquifers: Δg_w^c

Groundwater depletion in confined aquifers is the primary reason for land subsidence in Yunlin (Hung et al., 2021; Tran et al., 2022; Tsai and Hsu, 2018). Table 3 also shows the gravity changes contributed by groundwater changes in confined aquifers using Eq. 4. In Eq. 4, the storage coefficient (S) value and groundwater level change are required. However, in Table 1, there are just 4 out of 19 monitoring wells in different depths that had S values determined by pumping tests. To fulfill the requirement of estimating Δg_w^c, we first introduce trends in groundwater levels in our study sites in the middle fan and distal fan. By comparing their similarity in trends, we adopt a best S value for each monitoring well used in this study.

Like vertical displacements, groundwater level changes at the gravity sites are associated with precipitation variations. In the dry seasons, groundwater levels declined as a result of discharge due to a lack of sufficient precipitation. In general, groundwater levels started to rise in late May due to intensive precipitation, and thus May is the average month to start the wet season over CRAF and Taiwan (Fig. 8). Fig. 8 shows the relationship between groundwater level changes and precipitation at our gravity sites in the land subsidence-hit region in 2021. Fig. 8 shows all the groundwater levels monitored by the WRA used in this study. However, the depths and numbers of monitoring wells vary from one site to another. HLES and JJES are the only two stations where the groundwater levels of shallow aquifers (<30 m) are collected (Table 1). The rest of the monitoring wells are constructed in confined aquifers with JJES having the deepest depth (depth of screen) of 270 to 294 m.

Compared with groundwater level changes in a confined aquifer, those in a shallow unconfined aquifer above a confined aquifer can be much smaller because the magnitude of storage coefficients are different. For example, the groundwater level changes at depths 209 to 218 m (screen depths) is four times that at depths 13 to 31 m at HLES. However, we found daily groundwater records in shallow monitoring wells at HLES and JJES fluctuated more rapidly than those in deeper monitoring wells. The rapid water level fluctuations in the shallower aquifers might be due to frequent (daily) groundwater pumping from the shallow aquifers around HLES and JJES for irrigation (Chen et al., 2020). Note that no pumping tests were ever conducted for the shallow aquifers at HLES and JJES, thus no hydrogeological parameters such as S_y are available here. The patterns in groundwater fluctuations and sediment records in Fig. 2 suggest that the shallow aquifers at HLES and JJES are unconfined.

Storage coefficient values were lacking but necessary in groundwater modeling and gravity change estimation. The monitoring well at depths 95 to 104 m at JJES, i.e., JJES_D95–104 (Fig. 8a), was the only well with a storage coefficient value of 0.001167 (Table 1). Therefore, we assume that the monitoring well STES_D120–128 shares the same aquifer with JJES_D55–64, JJES_D95–104, TKJH_D54–84 and TKJH_D134–179, based on the similar pattern of groundwater level changes in these aquifers (Fig. 8a and the hydrogeology profile in Fig. 2). Therefore, the storage coefficient at STES_D120–128 was also 0.001167. Using this storage coefficient (0.001167) and the observed groundwater level change of 5.68 m, we estimate that Δg_w^c at STES_D120–128 on 23 September relative to 4 March 2021 is 0.3 μgal, which is only a fraction of the measured gravity change of 24 μgal. In addition, monitoring wells

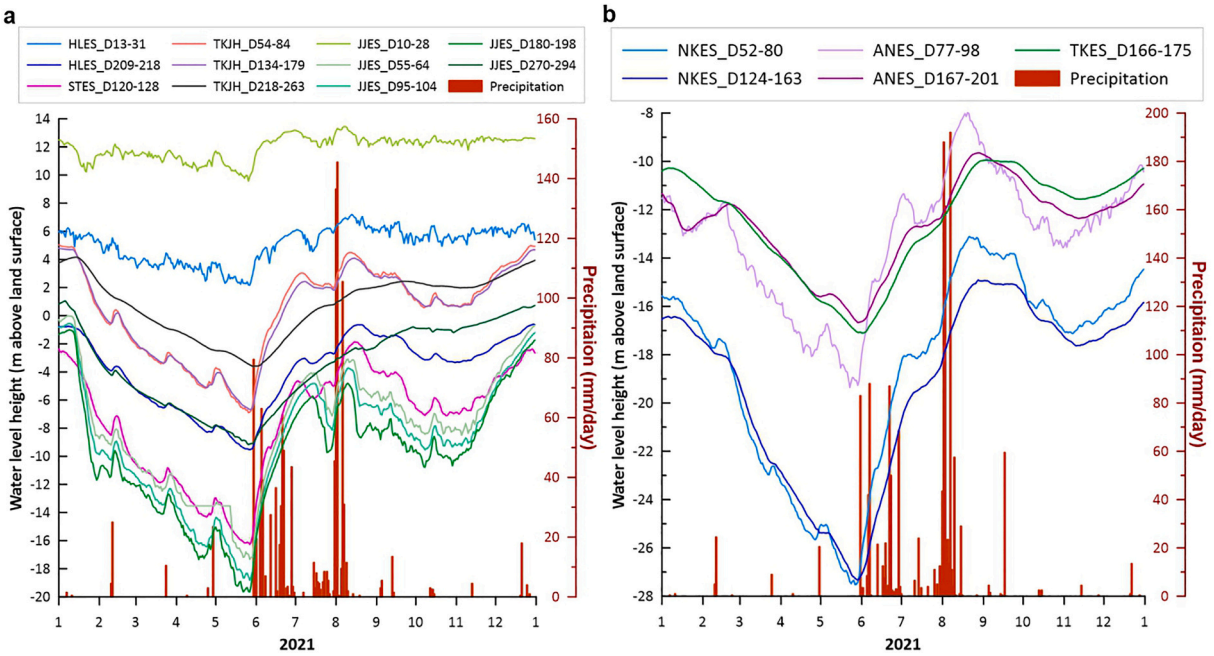

Fig. 8. Variations in groundwater level at the gravity sites located (a) in the middle fan and (b) in the land subsidence-hit region in the distal fan in 2021. The ranges of screen depths are shown following the station names. For example, HLES_D13–31 means that the range of screen depths is 13–31 m at station HLES. More information about groundwater monitoring wells is shown in Table 1.

of HLES_D209–218, TKJH_D218–263 and JJES_D270–294 may all be located in the third aquifer layer (F3 in Fig. 2). Because there was no pumping test conducted in this area at F3, we use the median value of S = 0.00025 at CRAF's middle fan to determine Δg_w^c, which is the gravity change due to the groundwater mass change in the confined aquifers at F3 in this study (Table 3).

Furthermore, we infer that the aquifer in the distal fan where ANES_D77–98 was installed was connected to NKES_D52–80 and NKES_D124–163, as shown in Fig. 8b. We use a storage coefficient value of 0.00298 (NKES_D52–80) to predict the gravity changes induced by the water storage changes from the confined aquifer F2. The same scenario is applied to ANES_D167–201 and TKES_D166–175. Note that TKES is close to NKES and is the closest site to ANES, where a storage coefficient value at depths around 160 to 200 m has been determined by a pumping test. Table 3 lists all the estimated gravity changes induced by water storage changes in confined aquifers (Δg_w^c) and induced by land subsidence.

5.4. Estimating retained groundwater in RUAs using residual gravity changes

Using the gravity changes and the method given in Section 4, we estimated retained groundwater volumes near our gravity sites. A residual gravity change is defined as the difference between a measured gravity change and the sum of the gravity changes due to vertical displacement and mass changes in confined aquifers (Δg_w^c) (Table 3). If the residual gravity changes at a site are significantly increased (larger than three times the typical one-μgal standard error of a mean gravity measurement, i.e., 3 μgal), they may imply retained groundwater is increased in a RUA around the site. However, more data are needed to determine the characteristics, dimensions and hydrogeological extensions of the RUA In Section 6.2, we will show that ERI can provide additional data about RUAs.

One of the RUAs studied in this paper is RUA1 near JJES. The residual gravity of the third measurement at JJES on 24 September 2021 increased by 14.2 μgal relative to the first gravity measurement on 15 March 2021. In this case, the estimated water storage change (ΔM_W^{JJES}) is 1454 ± 307 m^3 assuming an aquifer area of $A^{JJES} = \pi \times 37^2 = 4301$ m^2 (Eq. 6). In this case, the estimated $\sigma_{\Delta M_w}$ =307 m^3 is derived from Eq. (7) using the following values. First, $\sigma_{\Delta g} = \sqrt{1.0^2 + 1.8^2} = \pm 2.1$ μgal, based on the standard deviations of the absolute gravity values, which are 1.0 and 1.8 μgal on 24 September and 15 March 2021, respectively. Second, the vertical displacement (Δd) is 4.2 cm and its standard deviation ($\sigma_{\Delta d}$) is 1.0 cm; the latter is based on a standard deviation of 0.7 cm for the mean height in a day from the GNSS height measurements. Third, we use an approximate value of $R_{hg} = 2.0$ and assume that its standard deviation ($\sigma_{R_{hg}}$) is $= \pm 0.2$. The area A^{JJES} covers 90% of the area where the groundwater volume change between the two epochs (15 March 2021 and 24 September 2021) resulted in a difference in the gravity values as measured by the gravimeter at JJES. The area is assumed to be over a disk around JJES and its radius is ten times the groundwater level depth, i.e., 3.7 m, which was obtained from the water level records at the shallowest monitoring well (JJES_D10–28) on 24 September 2021; see Table 1. However, the extension of RUA1 below JJES (Fig. 2) can be larger than 4301 m^2. If the lithology, infiltration and recharge rates are all equal within RUA1, the groundwater volume retained in RUA1 could be several times larger than the estimated 4301 m^2.

The second studied RUA is RUA2 around STES, which could be extended to the gravity site HLES, as shown in Fig. 2. The monitoring well near STES has a screen opened at depths 120–128 m (F2, Table 1), where the hydraulic head changes might differ from those occurring in the shallow unconfined aquifer around STES. If we assume the groundwater levels at the shallowest monitoring well of HLES (HLES_D13–19, D22–31) were similar to those at STES, the groundwater level depth at STES was 8.0 m on 23 September 2021 (the third gravity measurement at STES). Using the residual gravity change of 23.6 μgal at STES, we estimate that $\Delta M_W^{STES} \approx 0.0238 \times 23.6 \times [\pi(80)^2] \approx 11{,}293 \pm 1483$ m^3. Like JJES, more data about the lithology, infiltration and recharge rates around STES are needed to estimate the actual groundwater volume accumulated in RUA2 around STES from March 2021 to September 2021. In summary, the residual gravity changes from March to September 2021 indicate significant increases in groundwater volume at RUA1 and RUA2 around JJES and STES, which differ from expected gravity changes that were mainly induced by land subsidence. In the

following sections, we will discuss the retained water between our gravity sites and the use of ERI techniques to clarify the extent of RUAs.

6. Discussions

6.1. Use of the estimated retained groundwater volumes for groundwater resource management

The estimated retained groundwater volumes (Section 5.4) in a specific period can contribute data to groundwater management in the subsidence-hit region of Yunlin. Such a gravity-based method is an alternative method for investigating groundwater storage changes, particularly at a regional spatial scale, compared with pointwise estimates based on groundwater water level changes and storage coefficient values from pumping tests (Chen et al., 2020). Fig. 9–11 shows gravity changes and their two separate contributions at each site located in the middle to distal fan. The first contribution is from vertical displacement (orange) and the second from groundwater storage change in a shallow regional unconfined aquifer (blue). The second contributions in Figs. 9–11 are derived from the residual gravity changes defined in Section 5.4 at all sites (Table 3).

Immediate accessibility of groundwater is the first concern when groundwater is used for agriculture and municipal water supplies. In general, little groundwater is needed when surface water is abundant over CRAF. For example, precipitation in Yunlin were plentiful in the first half-year in 2016, compared with the precipitation in the same period of 2021. Because such extra precipitation in 2016, relatively small amount of groundwater in Yunlin was pumped in 2016. The rain-groundwater use relationship is demonstrated by the gravity changes at TKJH for 2016 and 2021 (Fig. 9). In 2021, a drought year, groundwater was heavily pumped in the dry season, leading to a negative gravity change (Fig. 9b; May vs. March), despite the large land subsidence (8 cm) that should have produced a positive gravity change (the gravity change induced by vertical displacement is 16 μgal) as in 2016 (Fig. 9a). In March 2021, the gravity value was exceptionally low. As a result, the gravity measurement in September 2021 results in a relatively large gravity change (the third gravity change in Fig. 9b), which corresponds to a higher increase in water storage change in September 2021, compared with that in September 2016. Both the positive residual gravity changes in September 2016 and 2021 (relative to March) indicate the existence of RUAs that stored groundwater from the wet seasons of 2016 and 2021.

A large positive residual gravity change indicates a large groundwater volume change in a RUA. For example, Fig. 9a shows the residual gravity changes pat TKJH and HLES in 2016. The major difference is that the RUA around HLES stored more groundwater than TKJH right after the wet season (the third measurement) in 2016. Likewise, STES and JJES stored more groundwater than TKJH right after the wet season of 2021 (Fig. 10b and c). In particular, at the STES, >75% of gravity changes came from groundwater storage increases in the unconfined aquifer (RUA). In addition, although droughts occurred in the first half-year of 2021, the RUAs around STES and JJES can efficiently store groundwater in the wet season of 2021, as indicated by the relatively large residual gravity change in September 2021 (the third measurements/gravity changes in Fig. 10b,c). In terms of recharge efficiency, our gravity measurements indicate that STES is the best. Thus, it is recommended that a location near STES can be selected to construct an artificial recharge lake to mitigate land subsidence in the middle fan.

Some parts of the distal fan of CRAF also experience land subsidence (Fig. 1) and may need a recharge lake to replenish groundwater. Like Fig. 10, Fig. 11 explains how the information from our gravity measurements at NKES and ANES, located in the distal fan (Fig. 2), can assist the decision-making for a recharge lake. From Fig. 11, we conclude that NKES has a better recharge efficiency and is recommended as a potential recharge lake in the distal fan. This is explained as follows. The third gravity measurement at NKES (Fig. 11a) shows that the groundwater storage change contributed to a 24-μgal gravity increase, which is just 2.5 μgal less than that STES. This large gravity change at NKES indicates a high recharge efficiency. In comparison, the third gravity measurement in November 2021 at ANES shows only an 8-μgal gravity increase (no gravity measurement here in September 2021 due to a logistic problem).

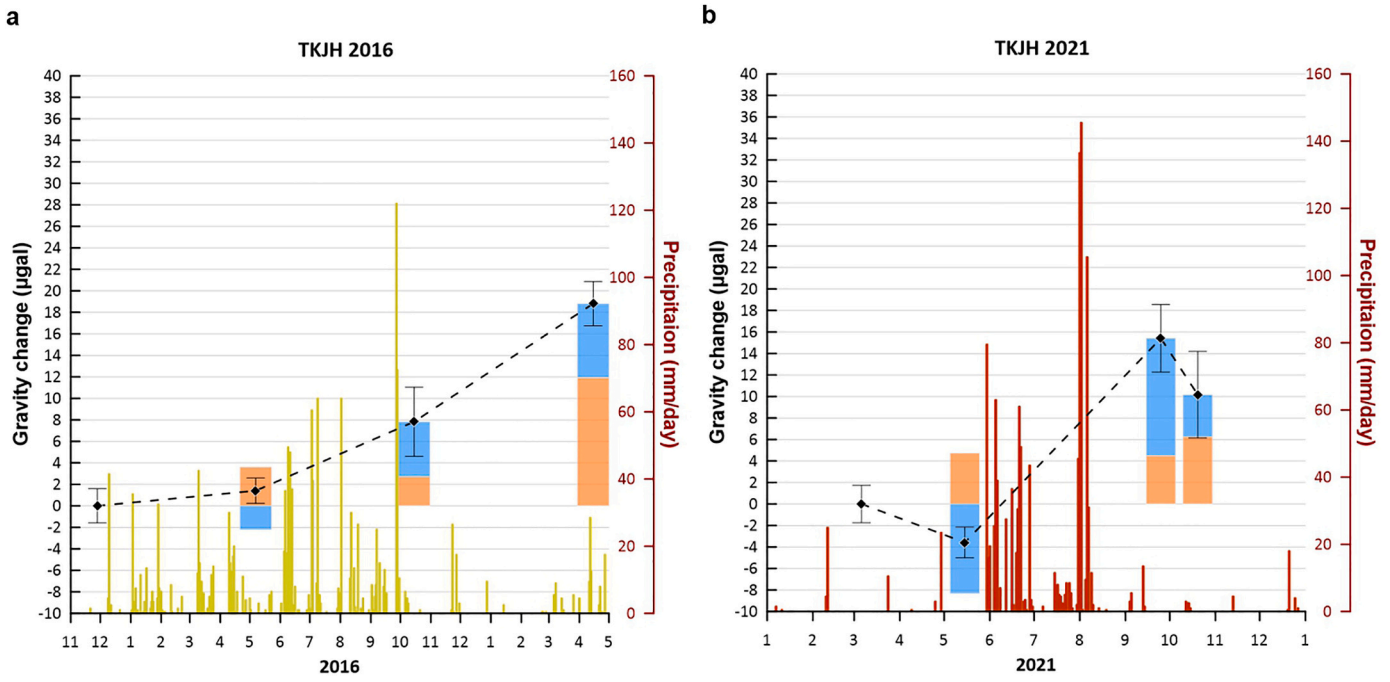

Fig. 9. Observed gravity changes at TKJH in 2016 and 2021. The gravity changes are divided into two contributions: (1) contribution induced by vertical displacement (orange). (2) contribution from water storage change in an unconfined aquifer (blue). A positive value in a contribution of water storage change means increased water storage relative to the first gravity measurement each year. A positive value in a contribution of vertical displacement means land subsidence which increases gravity value. (For interpretation of the references to colour in this figure legend, the reader is referred to the web version of this article.)

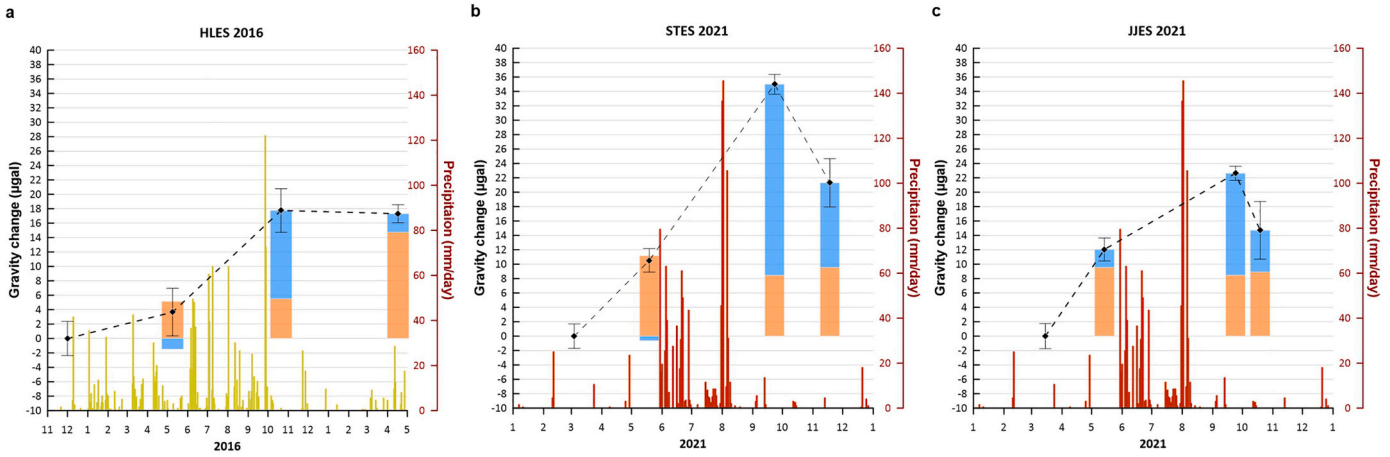

Fig. 10. Observed gravity changes with two gravity contributions (see Fig. 9) at (a) HLES in 2016, (b) STES and (c) JJES in 2021.

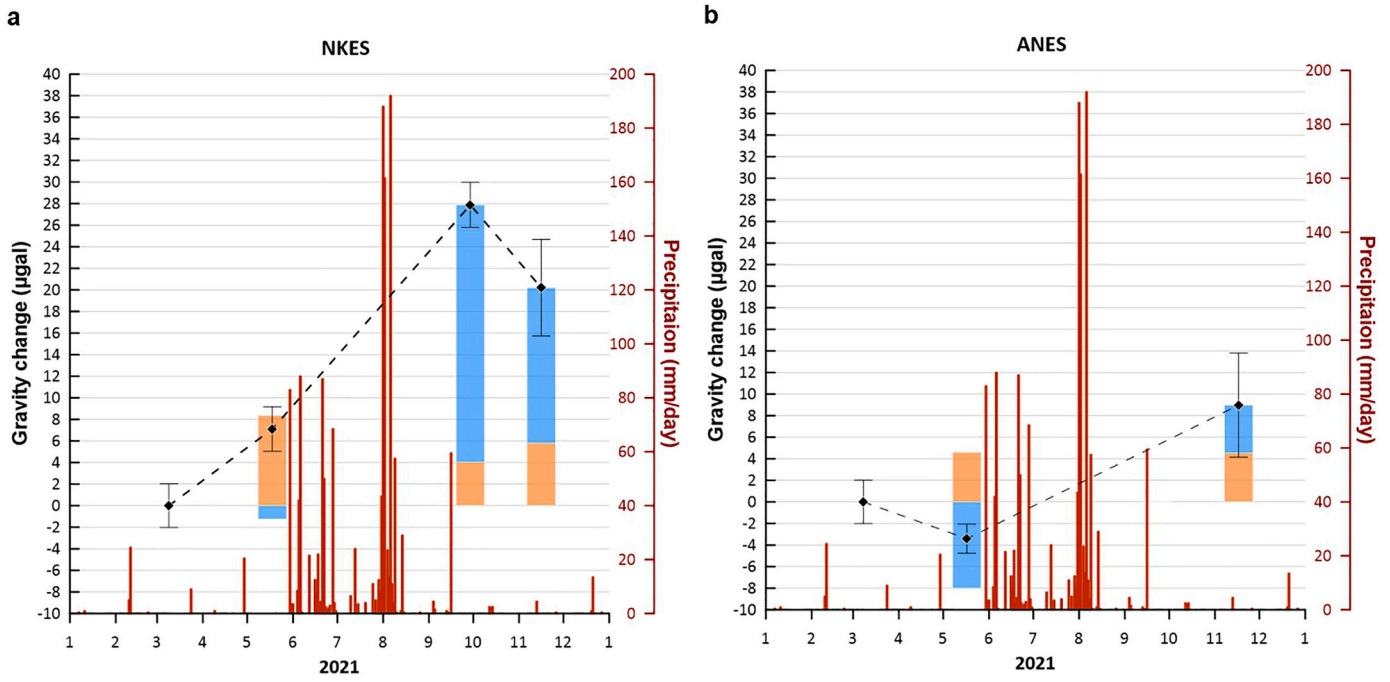

Fig. 11. Observed gravity changes and two gravity contributions (see Fig. 9) at (a) ANES and (b) NKES in the distal fan in 2021.

As explained earlier, 2021 is a drought year and is a year of high groundwater demand in Yunlin, especially in the dry season ending in May 2021. If a site is efficient for groundwater recharge, the gravity value after the wet season (in about September) should increase by a large amount, relative to the gravity value in March or May. The large gravity increase from third gravity measurements at NKES indicates that NKES stores much more groundwater than ANES after the wet season of 2021. Note that the residual gravity changes in Fig. 11 are relative to the first measurements, reflecting the groundwater storage changes since March 2021 in a limited region of the unconfined aquifer around gravity NKES or ANES. Additional data, such as those from the ERI method, are needed to clarify the exact areal extents of the aquifers and their capability to recharge and discharge groundwater.

6.2. Confirming RUAs by electrical resistivity imaging (ERI)

One sensor that can provide additional data about water storage changes around the two RUAs in Fig. 2 and the potential RUAs around NKES and ANES (Section 6.1) is ERI. Precise time-varying infiltration and recharge rates are most important parameters for a best estimate of water storage change (ΔM_w) over a RUA in Section 5.4, but obtaining these parameters can be challenging. In addition, the areal extension of a RUA is also a key factor in evaluating the potential of an artificial recharge lake. Recently, Chang et al. (2022) evaluated the potential of groundwater reservoir in the proximal fan of CRAF using ERI. ERI can estimate lithology and groundwater depth in a shallow unconfined aquifer. Fig. 12a shows the locations of ten interpreted ERIs conducted in May 2022, of which six ERIs are close to our gravity sites in the middle fan (Fig. 12b). Each ERI is 370 m in length with a 10-m electrode spaced by the Wenner–Schlumberger arrays. The ERI measurements were later inverted by the conjugated gradient method with the EarthImager™ 2D inversion software (AGI, 2003) and performed as the inverted images in Fig. 12. Fig. 12b shows four selected ERI images close to our gravity sites. Appendix shows the enlarged ten ERI images.

An ERI image shows the electrical resistivity as a function of depth along a profile. A relatively low resistivity (<50 Ohm-m) corresponds to

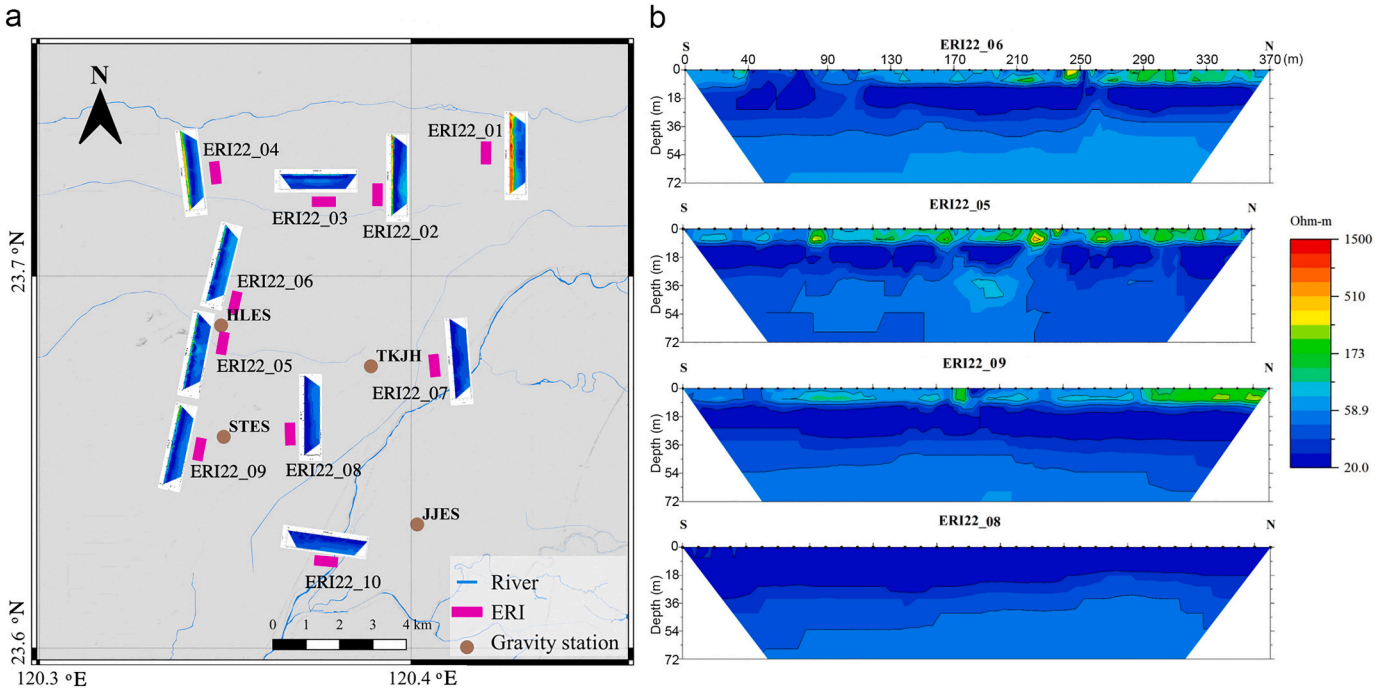

Fig. 12. (a) The locations (red lines) of the ERI images in CRAF (b) Four enlarged ERI images near gravity sites HLES (06 and 05), STES (09), and TKJH (08). An ERI image shows the electrical resistivity as a function of depth along a profile. A relatively low resistivity value (<50 Ohm-m) indicates clay sediments. (For interpretation of the references to colour in this figure legend, the reader is referred to the web version of this article.)

clay in a profile. ERI22_06, ERI22_05 and ERI22_09 in Fig. 12b are near HLES and STES. ERI22_09 is 800 m southwest of the STES gravity site and ERI22_05 is 1000 m southeast of the HLES gravity site (near RUA2 on the left in Fig. 2). With regions of relatively high resistivity above 10 m depth, the ERI images of ERI22_05, ERI22_06 and ERI22_09 confirm that the HLES and STES gravity sites are over sandy aquifers. That is, the image of ERI22_08 (located in the southeast of TKJH) indicates that here the surface layers contain only clay, and this is consistent with the expected location with clay shown near "TKJH" in Fig. 2. Unlike the ERI images near HLES and STES, the image of ERI22_08 does not show a recharge potential near the site of this image.

The ERI results partially agree with the hydrogeological profile in Fig. 2. ERI22_08 shows low resistivity values of 30–50 Ohm-m (clay) from depth 0 to 72 m, compared with the high resistivity values of 50–150 Ohm-m from depth 0 to 10 m along ERI22_06, ERI22_05, indicating the existence of fine sand. Below the 10-m depth of ERI22_06, ERI22_05 and ERI22_09, the resistivity values drop to below 50 Ohm-m, indicating increasing presence of clay like the profile of ERI22_08. In addition, the ERI images along ERI22_07 and ERI22_10 are similar to that along ERI22_08, suggesting that the discontinuity of the clay layer in the middle fan and unconfined aquifer are regional. The average depth of the RUAs revealed by the ERI images is about10 m, which is more specific than the rough depths estimated along the hydrogeological profile in Fig. 2. The more precise RUA depth estimations highlight the advantage of ERI over other sensors.

Both gravimetry and ERI are non-intrusive sensors. The discussion in this section shows they can work together to examine the areal extensions and the depths of the RUAs in the land subsidence-hit region of Yunlin, providing data for subsidence-mitigation engineering works such as constructions of recharge lakes. A recommended strategy for investigating a RUA is that a gravimetry study of the RUA is carried out first, followed by an ERI study. Gravimetry can sense large gravity changes between the dry and wet seasons of a RUA, but it alone cannot determine the RUA's depth and areal extent, which can be estimated by ERI. A joint use of gravimetry and ERI will benefit the construction of an artificial recharge lake near a RUA.

7. Conclusions

Land subsidence over CRAF is a pressing issue in Taiwan because the ongoing severe land subsidence may damage some segments of the Taiwan High Speed Rail in Yunlin to affect the rail's safety. Since groundwater pumping may have caused the large land subsidence rates in Yunlin, replenishing groundwater through RUAs may mitigate the subsidence problem. Using time-lapsed gravity measurements in the land subsidence-hit region, we identified two potential RUAs and estimated the retained groundwater volumes of the RUAs after the wet seasons, which can supply additional data for an efficient water resource management and effective constructions of recharge lakes. The gravity-based method for RUA identification and groundwater volume change estimate is non-intrusive, requiring little infrastructure to support the operation of the gravimeter.

It is recommended that additional tools, such as ERI, can be employed to collect data to clarify the areal extents and depths of the RUAs identified by the gravity-based method. Specifically, to explore the hydrogeological properties of a potential RUA, first a simple gravity site can be installed near the RUA to at least measure a gravity value in the dry season and another in the end of the wet season. If the difference between the two gravity values (without land subsidence gravity effect) is sufficiently large (see our numerical examples in Section 5.1), the RUA is likely to exist. The next investigation can be made using ERI, which examines how big and how deep the RUA can be.

Author contribution

KH Chen and C Hwang designed the experiments in the paper and wrote the manuscript. C Hwang is the project PI. Y Tanaka and CP Chang commented on the work in the paper and polished the manuscript. CP Chang provided the ERI images.

Author statements

This is an original paper and is not submitted to other jounals.

Declaration of Competing Interest

The authors declare there is no conflict of interest.

Data availability

Data will be made available on request.

Acknowledgments

This study is supported by the Ministry of Science and Technology, Taiwan, under Grants 110-MOEA-M-008-001, 111-MOEA-M-008-001, 110-2917-I-564-027 and 109-2221-E-009-015-MY3 and the Central Geological Survey, Taiwan, under Grants 111-5726901000-05-01. We thank the Editors and two anonymous reviewers for their comments that helped to improve this paper. All the gravity data used in this study are freely available at http://space.cv.nctu.edu.tw/publications/#data. KH Chen's postdoctoral research in the University of Tokyo is supported by the Ministry of Science and Technology, Taiwan.

Appendix A. Appendix

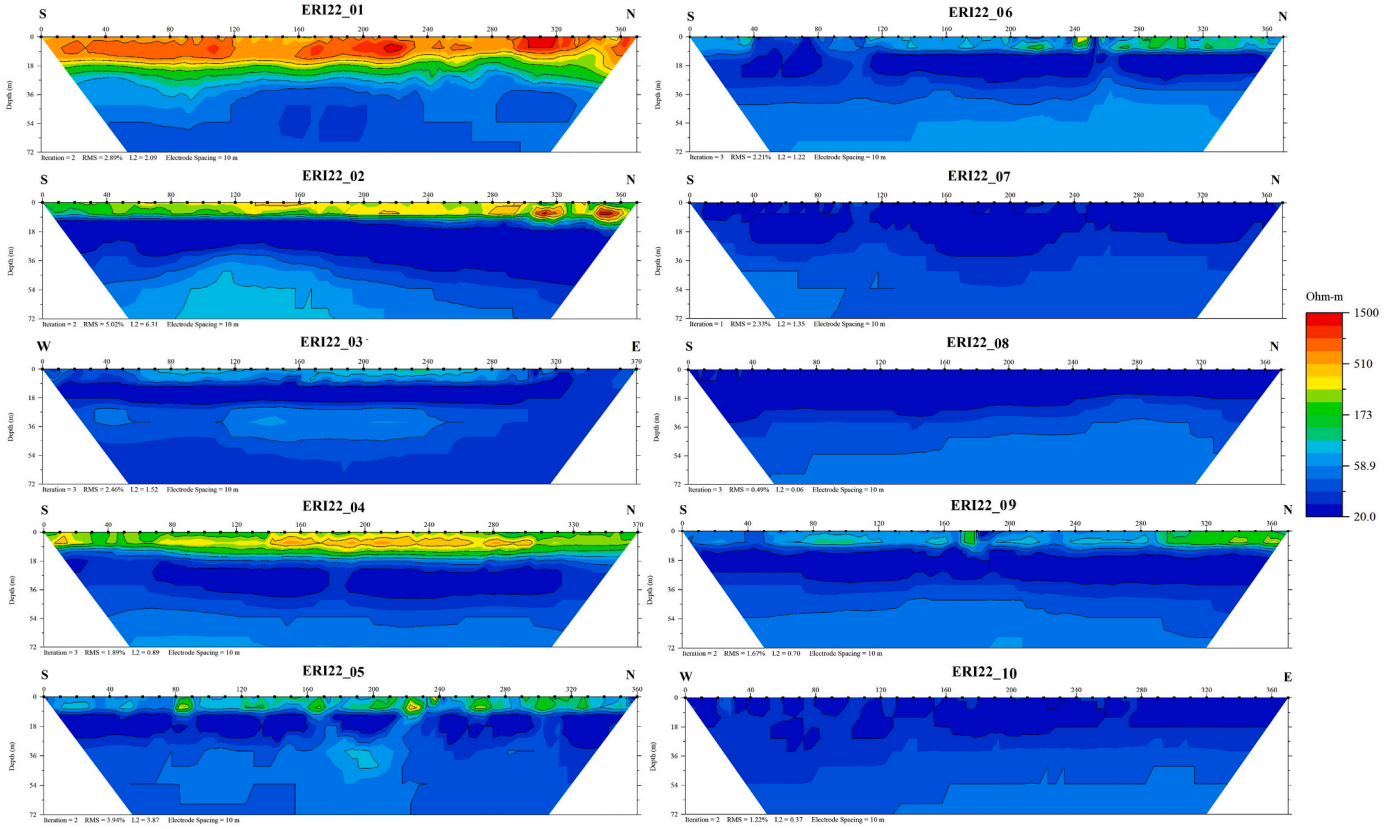

The enlarged 10 ERI images for supplementing the information in Fig. 12a.

References

AGI, 2003. Earth Imager 2D Resistivity Inversion Software, Version 1.5.10. Advanced Geosciences, Inc, Austin, TX.

Beattie, A., Ahmed, M., Haley, M., Rizzo, J., 2021. Quantifying land subsidence in the Coastal Bend of Texas using temporal gravity measurements. First Intern. Meet. Appl. Geosci. Energy Expand. Abst. 870–873. https://doi.org/10.1190/segam2021-3594938.1.

Central Geological Survey, 1999. Project of Ground-water Monitoring Network in Taiwan during the first stage: research report of Choushui River Alluvial Fan (in Chinese).

Chang, P.Y., Chang, L.C., Hsu, S.Y., Tsai, J.P., Chen, W.F., 2017. Estimating the hydrogeological parameters of an unconfined aquifer with the time-lapse resistivity-imaging method during pumping tests: Case studies at the Pengtsuo and Dajou sites, Taiwan. J. Appl. Geophys. 144, 134–143. https://doi.org/10.1016/j.jappgeo.2017.06.014.

Chang, P.-Y., Puntu, J.M., Lin, D.-J., Yao, H.-J., Chang, L.-C., Chen, K.-H., Lu, W.-J., Lai, T.-H., Doyoro, Y.G., 2022. Using Time-Lapse Resistivity Imaging Methods to Quantitatively Evaluate the potential of Groundwater Reservoirs. Water 14 (3). https://doi.org/10.3390/w14030420.

Chen, K.H., Hwang, C., Chang, L.C., Ke, C.C., 2018. Short-Time geodetic determination of aquifer storage coefficient in Taiwan. J. Geophys. Res.-Sol. Ea 123 (12), 10987–11015. https://doi.org/10.1029/2018jb016630.

Chen, K.H., Hwang, C., Chang, L.C., Tsai, J.P., Yeh, T.C.J., Cheng, C.C., Ke, C.C., Feng, W., 2020. Measuring aquifer specific yields with absolute Gravimetry: result in the Choushui River Alluvial Fan and Mingchu Basin, Central Taiwan. Water Resour. Res. 56 (9) https://doi.org/10.1029/2020WR027261.

Chen, K.H., Hwang, C., Chang, L.C., Tanaka, Y., 2021b. Infiltration coefficient, percolation rate and depth-dependent specific yields estimated from 1.5 years of absolute gravity observations near a recharge lake in Pingtung, Taiwan. J. Hydrol. 603, 127089 https://doi.org/10.1016/j.jhydrol.2021.127089.

Chen, Y.-A., Chang, C.-P., Hung, W.-C., Yen, J.-Y., Lu, C.-H., Hwang, C., 2021a. Space-Time Evolutions of Land Subsidence in the Choushui River Alluvial Fan (Taiwan) from Multiple-Sensor Observations. Remote Sens. 13 (12) https://doi.org/10.3390/rs13122281.

Crossley, D.J., Murphy, J.T., Liang, J., 2023. Comprehensive analysis of superconducting gravimeter data, GPS, and hydrology modelling in support of lunar laser ranging at Apache Point Observatory, New Mexico. Geophys. J. Int. 232, 1031–1065. https://doi.org/10.1093/gji/ggac357.

de Linage, C., Hinderer, J., Boy, J.-P., 2009. Variability of the Gravity-to-Height Ratio Due to Surface Loads. Pure Appl. Geophys. 166, 1217–1245. https://doi.org/10.1007/s00024-004-0506-0.

De Linage, C., Hinderer, J., Rogister, Y., 2007. A search for the ratio between gravity variation and vertical displacement due to a surface load. Geophys. J. Int. 171, 986–994. https://doi.org/10.1111/j.1365-246X.2007.03613.x.

Dietrich, S., Carrera, J., Weinzettel, P., Sierra, L., 2018. Estimation of specific Yield and its Variability by Electrical Resistivity Tomography. Water Resour. Res. 54 (11), 8653–8673. https://doi.org/10.1029/2018wr022938.

Fukuda, Y., Nishijima, J., Sofyan, Y., Taniguchi, M., Yusuf, M., Abidin, H.Z., 2016. Application of A10 Absolute Gravimeter for Monitoring Land Subsidence in Jakarta, Indonesia, International Symposium on Geodesy for Earthquake and Natural Hazards (GENAH). Springer International Publishing, Cham, pp. 127–134.

Hinderer, J., Hector, B., Riccardi, U., Rosat, S., Boy, J.P., Calvo, M., Littel, F., Bernard, J. D., 2020. A study of the monsoonal hydrology contribution using a 8-yr record (2010-2018) from superconducting gravimeter OSG-060 at Djougou (Benin, West Africa). Geophys. J. Int. 221 (1), 431–439. https://doi.org/10.1093/gji/ggaa027.

Hung, W.C., Hwang, C., Sneed, M., Chen, Y.A., Chu, C.H., Lin, S.H., 2021. Measuring and Interpreting Multilayer Aquifer-System Compactions for a Sustainable Groundwater-System Development. Water Resour. Res. 57 (4) https://doi.org/10.1029/2020WR028194.

Hung, W.-C., Hwang, C., Liou, J.-C., Lin, Y.-S., Yang, H.-L., 2012. Modeling aquifer-system compaction and predicting land subsidence in Central Taiwan. Eng. Geol. 147-148, 78–90. https://doi.org/10.1016/j.enggeo.2012.07.018.

Hwang, C., Kao, R., Cheng, C.C., Huang, J.F., Lee, C.W., Sato, T., 2009. Results from parallel observations of superconducting and absolute gravimeters and GPS at the Hsinchu station of Global Geodynamics Project, Taiwan. J. Geophys. Res.-Sol. Ea 114 (B7). https://doi.org/10.1029/2008jb006195.

Hwang, C., Cheng, T.C., Cheng, C.C., Hung, W.C., 2010. Land Subsidence using absolute and Relative Gravimetry: a Case Study in Central Taiwan. Surv. Rev. 42 (315), 27–39. https://doi.org/10.1179/003962609x451672.

Kao, R., Hwang, C.W., Kim, J.W., Ching, K.E., Masson, F., Hsieh, W.C., Le Moigne, N., Cheng, C.C., 2017. Absolute gravity change in Taiwan: present result of geodynamic process investigation. Terr. Atmos. Ocean. Sci. 28, 855–875. https://doi.org/10.3319/Tao.2017.06.13.01.

Kennedy, J., Ferre, T.P.A., Guntner, A., Abe, M., Creutzfeldt, B., 2014. Direct measurement of subsurface mass change using the variable baseline gravity gradient method. Geophys. Res. Lett. 41 (8), 2827–2834. https://doi.org/10.1002/2014gl059673.

Kennedy, J., Ferre, T.P.A., Creutzfeldt, B., 2016. Time-lapse gravity data for monitoring and modeling artificial recharge through a thick unsaturated zone. Water Resour. Res. 52 (9), 7244–7261. https://doi.org/10.1002/2016wr018770.

Kennedy, J., Rodriguez-Burgueno, J.E., Ramirez-Hernandez, J., 2017. Groundwater response to the 2014 pulse flow in the Colorado River Delta. Ecol. Eng. 106, 715–724. https://doi.org/10.1016/j.ecoleng.2016.10.072.

Landerer, F.W., Flechtner, F.M., Save, H., Webb, F.H., Bandikova, T., Bertiger, W.I., Bettadpur, S.V., Byun, S.H., Dahle, C., Dobslaw, H., Fahnestock, E., Harvey, N., Kang, Z., Kruizinga, G.L.H., Loomis, B.D., McCullough, C., Murböck, M., Nagel, P., Paik, M., Yuan, D.N., 2020. Extending the global mass change data record: GRACE follow-on instrument and science data performance. Geophys. Res. Lett. 47 (12) https://doi.org/10.1029/2020gl088306.

Lu, C.Y., Hu, J.C., Chan, Y.C., Su, Y.F., Chang, C.H., 2020. The relationship between surface displacement and groundwater level change and its hydrogeological implications in an Alluvial Fan: Case Study of the Choshui River, Taiwan. Remote Sens. 12 (20) https://doi.org/10.3390/rs12203315.

Mouyen, M., Simoes, M., Mouthereau, F., Masson, F., Hwang, C., Cheng, C.C., 2014. Investigating possible gravity change rates expected from long-term deep crustal processes in Taiwan. Geophys. J. Int. 198, 187–197. https://doi.org/10.1093/gji/ggu133.

Mouyen, M., Steer, P., Chang, K.J., Le Moigne, N., Hwang, C., Hsieh, W.C., Jeandet, L., Longuevergne, L., Cheng, C.C., Boy, J.P., Masson, F., 2020. Quantifying sediment mass redistribution from joint time-lapse gravimetry and photogrammetry surveys. Earth Surf. Dynam. 8 (2), 555–577. https://doi.org/10.5194/esurf-8-555-2020.

Pool, D.R., 2008. The utility of gravity and water-level monitoring at alluvial aquifer wells in southern Arizona. Geophysics 73 (6), Wa49-Wa59. https://doi.org/10.1190/1.2980395.

Reich, M., Mikolaj, M., Blume, T., Guntner, A., 2019. Reducing gravity data for the influence of water storage variations beneath observatory buildings. Geophysics 84 (1), En15-En31. https://doi.org/10.1190/Geo2018-0301.1.

Rosat, S., Hinderer, J., 2018. Limits of detection of gravimetric signals on earth. Sci. Rep. 8 (1), 15324. https://doi.org/10.1038/s41598-018-33717-z.

Schwartz, F.W., Zhang, H., 2002. Fundamentals of Groundwater Hydrology. Wiley, New York.

Tanaka, Y., Suzuki, T., Imanishi, Y., Okubo, S., Zhang, X.L., Ando, M., Watanabe, A., Saka, M., Kato, C., Oomori, S., Hiraoka, Y., 2018. Temporal gravity anomalies observed in the Tokai area and a possible relationship with slow slips. Earth Planets Space 70. https://doi.org/10.1186/s40623-018-0797-5.

Tapley, B.D., Bettadpur, S., Watkins, M., Reigber, C., 2004. The gravity recovery and climate experiment: Mission overview and early results. Geophys. Res. Lett. 31 (9) https://doi.org/10.1029/2004gl019920.

Torge, W., 1989. Gravimetry. Walter de Gruyter, Berlin.

Tran, D.-H., Wang, S.-J., Nguyen, Q.C., 2022. Uncertainty of heterogeneous hydrogeological models in groundwater flow and land subsidence simulations – a case study in Huwei Town, Taiwan. Eng. Geol. 298 https://doi.org/10.1016/j.enggeo.2022.106543.

Tsai, J.P., Yeh, T.C.J., Cheng, C.C., Zha, Y.Y., Chang, L.C., Hwang, C.W., Wang, Y.L., Hao, Y.H., 2017. Fusion of Time-Lapse Gravity Survey and Hydraulic Tomography for estimating Spatially varying Hydraulic Conductivity and specific Yield Fields. Water Resour. Res. 53 (10), 8554–8571. https://doi.org/10.1002/2017wr020459.

Tsai, M.-S., Hsu, K.-C., 2018. Identifying poromechanism and spatially varying parameters of aquifer compaction in Choushui River alluvial fan, Taiwan. Eng. Geol. 245, 20–32. https://doi.org/10.1016/j.enggeo.2018.07.025.

Van Camp, M., de Viron, O., Watlet, A., Meurers, B., Francis, O., Caudron, C., 2017. Geophysics from terrestrial time-variable gravity measurements. Rev. Geophys. 55 (4), 938–992. https://doi.org/10.1002/2017rg000566.

Wang, J., Shen, C., Xuan, S., Wu, G., Sun, K., 2021. Rigorous Evaluation of Gravity Change due to Crustal Vertical Deformation. Pure Appl. Geophys. 178, 2077–2089. https://doi.org/10.1007/s00024-021-02742-x.

Watlet, A., Van Camp, M., Francis, O., Poulain, A., Rochez, G., Hallet, V., Quinif, Y., Kaufmann, O., 2020. Gravity monitoring of underground flash flood events to study their impact on groundwater recharge and the distribution of Karst Voids. Water Resour. Res. 56 (4) https://doi.org/10.1029/2019wr026673.

Yang, Y.J., Hwang, C., Hung, W.C., Fuhrmann, T., Chen, Y.A., Wei, S.H., 2019. Surface deformation from Sentinel-1A InSAR: relation to seasonal groundwater extraction and rainfall in Central Taiwan. Remote Sens. 11 (23) https://doi.org/10.3390/rs11232817.

Zerbini, S., Richter, B., Rocca, F., van Dam, T., Matonti, F., 2007. A combination of space and terrestrial geodetic techniques to monitor land subsidence: case study, the southeastern Po Plain, Italy. J. Geophys. Res.-Sol. Ea 112 (B5). https://doi.org/10.1029/2006jb004338.